TITLE: The *Acinetobacter baumannii* Mla system and glycerophospholipid transport to the outer membrane

AUTHORS: Cassandra Kamischke[1], Junping Fan[1], Julien Bergeron[4,5], Hemantha D. Kulasekara[1], Zachary D. Dalebroux[1], Anika Burrell[4], Justin M. Kollman[4] and Samuel I. Miller[1,2,3*]

AFFILIATIONS:

[1]Departments of Microbiology, [2]Genome Sciences, [3]Medicine, and [4]Biochemistry, University of Washington, Seattle, WA. [5]Department of Molecular Biology and Biotechnology, The University of Sheffield.

*Correspondence to: millersi@uw.edu

ABSTRACT

The outer membrane (OM) of Gram-negative bacteria serves as a selective permeability barrier that allows entry of essential nutrients while excluding toxic compounds, including antibiotics. The OM is asymmetric and contains an outer leaflet of lipopolysaccharides (LPS) or lipooligosaccharides (LOS) and an inner leaflet of glycerophospholipids (GPL). We screened *Acinetobacter baumannii* transposon mutants and identified a number of mutants with OM defects, including an ABC transporter system homologous to the Mla system in *E. coli.* We further show that this opportunistic, antibiotic-resistant pathogen uses this multicomponent protein complex and ATP hydrolysis at the inner membrane to promote GPL export to the OM. The broad conservation of the Mla system in Gram-negative bacteria suggests the system may play a conserved role in OM biogenesis. The importance of the Mla system to *Acinetobacter baumannii* OM integrity and antibiotic sensitivity suggests that its components may serve as new antimicrobial therapeutic targets.

INTRODUCTION

Gram-negative bacteria are enveloped by two lipid bilayers, separated by an aqueous periplasmic space containing a peptidoglycan cell wall. The inner membrane (IM) is a symmetric

bilayer of glycerophospholipids (GPL), of which zwitterionic phosphatidylethanalomine (PE), acidic phosphatidylglycerol (PG), and cardiolipin (CL) are among the most widely distributed in bacteria (1). In contrast, the outer membrane (OM) is largely asymmetric and composed of an inner leaflet of GPL and an outer leaflet of lipopolysaccharide (LPS) or lipooligosaccharide (LOS) (2). The OM forms the first line of defense against antimicrobials by functioning as a molecular permeability barrier. The asymmetric nature of its lipid bilayer and the structure of LPS/LOS molecules facilitates barrier function, as the core region of LPS impedes the entry of hydrophobic molecules into the cell while the acyl chains within the bilayer also help to prevent the entry of many hydrophilic compounds (3). Although progress has been made in understanding many aspects of OM assembly – including the discovery of an LPS transport system and the machinery for proper folding and insertion of outer membrane proteins (4, 5) – little is known about the molecular mechanisms for transport of the GPLs necessary for OM formation and barrier function.

Acinetobacter baumannii is an important cause of antibiotic-resistant opportunistic infections and has significant innate resistance to disinfectants and antibiotics. Similar to other Gram-negative opportunistic pathogens such as *Pseudomonas aeruginosa* and *Klebsiella* spp., individuals with breached skin or damaged respiratory tract mucosa are most vulnerable (6, 7). We performed a genetic screen to identify genes important for the OM barrier of *A. baumannii*. This led to the identification of an ABC (ATP-binding cassette) transporter complex that promotes GPL export to the OM. Transporter disruption attenuates bacterial OM barrier function, resulting in increased susceptibility of *A. baumannii* to a wide variety of antibiotics.

The homologous system for *E. coli* has previously been termed Mla for its suggested role in the maintenance of outer membrane lipid asymmetry via the removal of GPL from the outer leaflet of the OM to the IM. While this is a reasonable hypothesis, there is not direct biochemical evidence that the Mla system functions to return GPL from the OM to the IM. In this work, we present evidence that the *A. baumannii* Mla system functions to promote GPL movement from the IM to the OM. This conclusion is based on the observation that newly synthesized GPLs accumulate at the IM of *mla* mutants, akin to how LPS molecules accumulate at the inner membrane in bacteria with mutations in the *lpt* genes encoding the LPS ABC transport system (5). Given the broad conservation of Mla in prokaryotic diderm organisms, the anterograde trafficking function of Mla might be exploited by a variety of species.

RESULTS

A screen for activity of a periplasmic phosphatase identifies genes required for *A. baumannii* OM barrier function.

We identified strains with mutations in genes required for maintenance of the *Acinetobacter baumannii* OM barrier by screening transposon mutants for the development of a blue colony phenotype on agar plates containing the chromogenic substrate BCIP-Toluidine (XP). Although *A. baumannii* carries an endogenous periplasmic phosphatase enzyme, colonies remain white on agar plates containing XP. We reasoned that lesions in genes necessary for the OM barrier function should result in a blue colony phenotype, as the XP substrate becomes accessible to the periplasmic enzyme (8, 9). Screening roughly 80,000 transposon-containing colonies for the blue colony phenotype yielded 364 blue colonies whose insertions were mapped to 58 unique genes (Supplemental File 1). We confirmed the results of the screen by assaying for OM-barrier defects using ethidium bromide (EtBr) and N-Phenyl-1-naphthylamine (NPN) uptake assays (10, 11). We also tested for resistance to antimicrobials, including trimethoprim, rifampicin, imipenem, carbenicillin, amikacin, gentamicin, tetracycline, polymyxin B, and erythromycin. Greater than 85% of the strains identified in the screen demonstrated decreased OM barrier function compared to wild type. Out of the 58 strains with transposon insertions, 23 demonstrated OM permeability defects by NPN and EtBr uptake assays, and 49 out of 58 resulted in increased sensitivity to two or more antibiotics compared to the parent strain, indicating that the screen identified lesions causing OM barrier defects leading to increased permeability to small charged and hydrophobic molecules, including commonly used antibiotics.

The Mla system is necessary for *A. baumannii* OM integrity

Four mutants with a blue colony phenotype contained unique transposon insertions in the genetic loci A1S_3103 and A1S_3102, predicted to encode core components (*mlaF* and *mlaE*) of a multicomponent ABC transport system. These genes are within a five-gene operon that encodes for a conserved proteobacterial ABC transport system homologous to the *E. coli mla* system previously implicated in OM integrity (12). The *A. baumannii* operon includes: *mlaF* and *mlaE,* respectively predicted to encode the nucleotide-binding and transmembrane domains of an ABC transporter; *mlaD,* encoding a protein containing an IM-spanning domain and a predicted

periplasmic soluble domain; *mlaC,* encoding a soluble periplasmic protein; and *mlaB,* an additional gene predicted to encode a cytoplasmic sulfate transporter and anti-sigma factor antiagonist (STAS)-domain protein (Figure 1A). An additional putative OM lipoprotein is encoded on *mlaA*, or *vacJ,* which is clustered with the rest of the *mla* operon in some Gram-negative bacteria, although it is at a different chromosomal location in *A. baumannii*. MlaA has been functionally associated with the rest of the Mla components in *E. coli*, as mutations in *mlaA* yield comparable phenotypes to mutations in other components of the system (8).

Bioinformatic analysis predicts that the *mlaC* and *mlaF* genes respectively encode the soluble periplasmic component and cytoplasmic ATPase component of the ABC transport system, and we chose to focus on mutants of these genes for further experiments to elucidate the function of the *mlaFEDCB* operon. Chromosomal deletions were created by allelic exchange, and these mutations resulted in OM permeability defects as measured by EtBr uptake assays. We complemented the OM defect for the Δ*mlaC* and Δ*mlaF* deletion mutants by repairing the original deletion event in the chromosome and confirmed complementation of the observed permeability defect (Figure 1B). Deletions in *mlaF* and *mlaC* also rendered *A. baumannii* increasingly sensitive to a variety of antibiotics as determined by MIC measurements (Figure 1D). Increased sensitivity to antibiotics whose uptake is not mediated by OM porins is consistent with a direct effect on the membrane component of the OM permeability barrier (13, 14). In addition to OM defects, the *mla* mutants display phenotypes that may correlate with OM stress, including increased production of extracellular carbohydrates as evidenced by crystal violet staining of pellicles following growth in broth culture (Figure 1 – figure supplement 1A). These data indicate a role for Mla in the maintenance of the outer membrane barrier of *A. baumannii*.

ATPase activity of MlaF is required for maintenance of the OM barrier of *A. baumannii*

To exclude the possibility that the membrane defect was the result of the disruptive effect of a partially formed Mla protein complex, we engineered an enzymatically inactive ATPase component and expressed the defective enzyme from a plasmid. We reasoned that by expressing this allele in the wild type bacteria we could create a dominant-negative effect on Mla function. The cytoplasmic ATPase component of the Mla system, MlaF, contains the consensus sequence GxxxxGKT at residues 49-56, characteristic of a Walker A motif. Downstream residues 173-178 contain the sequence LIMYDE, typical of a Walker B motif. The Walker motifs form highly

conserved structures critical for nucleotide binding and hydrolysis (15). The lysine residue of the Walker A motif is particularly essential for the hydrolysis of ATP. Mutations in this lysine residue are inhibited for nucleotide binding, and the mutated protein is rendered inactive (16). Additionally, ATPase mutants in the key lysine residue have been shown to have a dominant-negative effect on ATP hydrolysis when co-expressed with their wild-type ATPase counterparts, as typical ABC transporters have a structural requirement for two functional nucleotide-binding proteins which dimerize upon substrate transport (17, 18).

Therefore, we created a version of the MlaF coding sequence with a leucine substitution of the Walker A lysine residue ($MlaF^{K55L}$), and then cloned the mutated *mlaF* into the low-copy pMMBkan vector under control of the *mlaF* native promoter. We observed that expression of $MlaF^{K55L}$ in wild type *A. baumannii* had a dominant-negative effect on membrane permeability as measured by EtBr uptake (Figure 1C), and expression of $MlaF^{K55L}$ also resulted in increased exopolysaccharide production as demonstrated by increased staining by crystal violet (Figure 1 – figure supplement 1B). Correspondingly, expression of $MlaF^{K55L}$ rendered *A. baumannii* more sensitive to a variety of antibiotics, resulting in reduced MICs when compared to *A. baumannii* expressing the empty pMMBkan vector (Figure 1D). Therefore, expression of a defective ATPase results in a dominant-negative mutant with a comparable phenotype to deletion of components of the *mla* operon. These results demonstrate a requirement for ATP hydrolysis by MlaF for the maintenance of OM barrier function in *A. baumannii*, and indicate that the phenotypes of deletion mutants were likely a result of a lack of transport function, rather than formation of a toxic incomplete membrane protein complex.

Structure of the *A. baumannii* MlaBDEF complex

The genetic arrangement and conservation of the components of this ATPase-containing transport complex indicated it was likely that the individual components formed a higher order protein structure. To define whether the Mla components form a stable protein complex, we expressed the entire operon (*mlaFEDCB*) from *A. baumannii* ATCC 17978 in *E. coli* with a carboxy-terminal hexahistidine tag on the MlaB component. Affinity purification of MlaB revealed three additional bands, with sizes corresponding to MlaF, MlaD, and MlaE (Figure 2 – figure supplement 1) and confirmed by MALDI-TOF mass spectrometry analysis, indicating that these four proteins form a stable complex. We did not detect MlaC, suggesting it might interact

only transiently with the other components, consistent with results recently reported by Thong et al. (19).

We next used cryo-electron microscopy to characterize the architecture of the *A. baumannii* MlaBDEF complex (abMlaBDEF). This complex is uniformly dispersed in vitreous ice (Figure 2 – figure supplement 2A), and 2D classification demonstrated the presence of a range of views suitable for structure determination (Figure 2 – figure supplement 2B). Following 2D- and 3D-classification, we obtained a final dataset of ~ 14,000 particles with which we obtained a structure to a resolution of 8.7 Å (Figure 2 – figure supplement 2D). The structure possesses significant visible features in agreement with the nominal resolution (Figure 2 – figure supplement 2C). Based on the bioinformatically-predicted localization of individual proteins and work recently performed on the similar *E. coli* Mla complex *(*ecMlaBDEF*)* (19), we propose that MlaD localizes to the periplasmic side of the IM, MlaE forms the central transmembrane region, and MlaF and MlaB form the bottom layer on the cytoplasmic face of the IM with two visible hetero-dimers (Figure 2 – figure supplement 2E). We note that the structure of ecMlaBDEF, at lower resolution, was reported recently (20). The overall features of both structures, solved independently, are identical, suggesting that they correspond to the correct structure for the complex. However, the limited resolution of the ecMlaBDEF complex structure did not allow modeling of its individual subunits, in contrast to the abMlaBDEF structure reported here.

We note that a clear six-fold symmetry is present for the region of the map attributed to MlaD (Figure 2B), despite the fact that we only imposed a 2-fold symmetry averaging. This agrees with the proposed hexameric state of its *E. coli* homologue (ecMlaD) (19). We next modeled abMlaD, using an evolution restraints-derived structural model of ecMlaD (21) as a template, and used our previously-published EM-guided symmetry modeling procedure (22) to model its hexameric state. The obtained abMlaD hexameric model is at a low-energy minimum (Figure 2 – figure supplement 3B) and fits the EM map density well (Figure 2B and Figure 2 – figure supplement 4B). A crystal structure of the periplasmic domain of ecMlaD published recently (20) formed a crystallographic hexamer, suggesting that this corresponds to the native hexomeric arrangement for this domain. Our abMlaD hexameric model is very similar to the crystallographic ecMlaD structure (Figure 2 – figure supplement 3C), supporting the proposed domain arrangement in the MlaBDEF complex. We note, however, that one region of density in the EM map is not accounted for by our MlaD hexamer model (Figure 2B). The localization of

this extra density suggests that it corresponds to a ~ 45 amino-acid insert present between strands 4 and 5 of the abMlaD β-sheet (Figure 2 – figure supplement 4A). The role of this insert, uniquely found in the *A. baumannii* orthologue, is not known.

We next modeled the structures of MlaB and MlaF and fitted their respective coordinates in the corresponding region of the EM map (Figure 2C and Figure 2 – figure supplement 3A). For both proteins, most helices are well resolved, which allowed us to place the models unambiguously. We then compared the conformation of the ATPase MlaF to that of the maltose transporter ATPase MalK, which has been trapped in several conformations of the transporter; i.e. the inward-facing state, the pre-translocation state, and the outward-facing state (23, 24). Interestingly, the arrangement of MlaF clearly resembles the pre-translocation state of MalK (Figure 2D). This suggests that we have trapped a similar conformation of the abMlaBDEF complex. It is possible that MlaD and/or MlaF, for which there are no equivalent in other ABC transporters, stabilizes this conformation. Alternatively, it is possible that the presence of detergents, which were present to solubilize the complex, mimics the natural ligand in the transporter's active site. Finally, the transmembrane (TM) region of the map is well resolved, and density for the transmembrane (TM) helices can be clearly identified. We therefore modeled abMlaE, using an evolution restraints-derived structural model of ecMlaE (21) as a template, and fitted the obtained coordinates in the corresponding region of the map, with the orientation corresponding to the predicted topology. The resulting MlaE dimer model (Figure 2D) fits well to the EM map density (Figure 2 – figure supplement 4C), and clearly corresponds to a closed transporter, with no solvent channel between the subunits. Interestingly, we also noted clear density for three TM helices that likely correspond to the MlaD N-terminal helices (Figure 3A). However, they lacked continuity, and we observed that only two form a direct interaction with MlaE. It is possible that this is due to heterogeneity in the orientation of MlaD relative to the rest of the complex. To verify this, we performed further 2D classification of the particles used for reconstruction (Figure 3B), which revealed a range of positions for the MlaD region relative to the rest of the complex. We therefore performed further 3D classification leading to a smaller dataset of ~ 8,000 particles. This produced a structure of lower resolution (~ 11.5 Å) but with the six MlaD N-terminal TM helices clearly visible (Figure 3B). While the periplasmic domain possesses 6-fold symmetry, the TM domains of MlaD do not appear symmetrical, with two forming close contacts with the density attributed to MlaE while the other four do not appear to

contact any other proteins. This observation likely explains the asymmetry of contacts between the dimeric MlaE and the hexameric MlaD. A higher-resolution structure will be required to determine if additional contacts are formed between the outward-facing loops of MlaE and the periplasmic domain of MlaD.

Components of the Mla system interact directly with GPL

The crystal structure of MlaC has been solved from *Ralstonia solanacearum*. The structure contains a single phosphatidylethanolamine molecule oriented such that the hydrophobic acyl chains are located inside the protein while the hydrophilic head group is exposed (25). More recently, the crystal structure for MlaC has been solved from *E. coli* and shown to bind lipid tails (20). As noted in previous work performed on the *E. coli* Mla system, this is strong evidence that the substrates of the Mla system are GPL (12). In order to confirm that the periplasmic components of the Mla pathway in *A.baumannii* interact with GPL, we purified the soluble domains of both MlaC and MlaD by expressing histidine-tagged proteins followed by Ni-affinity FPLC purification. After overnight dialysis of the proteins, we performed Bligh-dyer chloroform extraction on the purified proteins to isolate any bound GPL and analyzed the results by LC-MS/MS. GPL analysis revealed both phosphatidylglycerol and phosphatidylethanolamine of varying acyl chain lengths. This suggests the possibility that the periplasmic substrate binding components of the system may bind diacylated GPL molecules with limited polar head group specificity (Figure 4 – figure supplement 1).

Mla mutants have decreased abundance of outer membrane GPL

Given the OM defect of *mla* mutants, as well as the system's apparent direct association with GPL, we chose to further characterize the overall membrane GPL composition of the *mla* mutants. Previous work on the Mla system in *E.coli* has demonstrated an increase in hepta-acylated lipid A in *mla* mutants, indicating activation of PagP that acylates GPL and lipid A in the outer leaflet of the OM in enterobacteria (12, 26). From this data it has been suggested that the system may serve to maintain lipid asymmetry within the OM, although it is well known that GPL displacement to the OM outer leaflet is a general reflection of chemical damage to the OM (27-29). However, biochemical analysis of the membrane GPL composition for *mla* mutants has not been published for any organism to our knowledge, so we sought to apply our lab's methods of GPL quantification to test the hypothesis of retrograde transport function. To determine

whether *A. baumannii mla* mutations cause changes in the membrane GPL concentration, GPL were extracted from inner and outer membrane fractions separated by density centrifugation. As can be seem on figure S11, density centrifugation results in nice separation of the outer and inner membranes of *Acinetobacter baumannii,* with the OM contain the vast majority of OmpA and the inner membrane containing all the NAPPH oxidase. Thin-layer chromatography (TLC) and electrospray-ionization time-of-flight mass spectrometry (ESI-MS) were used to qualitatively assess GPL composition from these well separated membrane fractions. TLC and ESI-MS indicated Δ*mlaC A. baumannii* had a dramatically decreased abundance of all major phospholipid species in the OM compared to wild type. (Figure 4A and Figure 4 – figure supplement 2).

To better analyze the differences in membrane GPL, we quantified GPL by normal phase liquid-chromatography collision-induced-dissociation mass spectrometry (LC-MS/MS). We quantified the ratio of individual GPL within each membrane by normalizing to an internal standard of known quantity. We then normalized the quantified GPL to the protein content of isolated IM and OM. Quantitative LC-MS/MS confirmed the overall reduction in outer membrane GPLs observed by ESI-MS and TLC, with the reduced levels observable across multiple GPL species for Δ*mlaC* mutants relative to wild type (Figure 4B). Therefore, mutations in the components of the Mla system result in a decrease in OM GPL, whereas the retrograde transport hypothesis would predict an increase in OM GPL. Therefore, these results instead suggest a possible role for Mla in outward GPL trafficking.

Mla mutants demonstrate an accumulation of newly synthesized GPL in the IM

The overall decrease in outer membrane glycerophospholipids of A. baumannii *mla* mutants suggests that either the Mla system is functioning to deliver GPLs from the inner membrane to the outer membrane, or alternatively, mutations in the Mla system may disrupt the outer membrane in a manner that leads to the activation of outer membrane phospholipases, which then degrade GPL. Work performed on the Mla system in *E.coli* has demonstrated that disruption of genes in the Mla pathway results in activation of both the OM acyl-transferase PagP, which cleaves a palmitate moiety from GPL and transfers it to LPS and PG , creating a hepta-acylated LPS molecule and palmitoyl-PG and the OM phospholipase PldA (12, 28). *A. baumannii* has no known PagP enzyme but similar activity of the multiple predicted OM

phospholipases could account for the reduction in OM GPL as observed by TLC and quantitative mass spectrometry. Therefore, we designed a mass spectrometry-based assay to study intermembrane GPL transport using ^{13}C stable isotope labeling (Figure 5 – figure supplement 1A), to better analyze the directionality of GPL transport by the Mla system between the bacterial membranes. When grown in culture with sodium acetate as the sole carbon source, many bacteria directly synthesize acetyl-CoA using the conserved enzyme acetyl-CoA synthase (30). Acetyl CoA, the precursor metabolite for fatty acid biosynthesis, is first converted to malonyl-CoA and enters the FasII (fatty acid biosynthesis) pathway that supplies endogenously synthesized fatty acids to macromolecules such as lipopolysaccharides, phospholipids, lipoproteins, and lipid-containing metabolites. By growing cultures in unlabeled acetate then "pulsing" with 2-^{13}C acetate and analyzing separated membrane fractions from set time points, we can observe the flow of newly synthesized GPLs between the IM and OM of *A. baumannii* (Figure 5 – figure supplement 1B) (26).

Upon introducing the 2-^{13}C acetate as the sole carbon source, ^{13}C-labeled GPL were immediately synthesized in the bacterial cytoplasm. We reasoned that continued growth in ^{13}C acetate should result in a mixed pool of unlabeled and labeled IM GPL molecules. As the GPL are then fluxed from the IM to the OM, the likelihood that an individual GPL molecule is transported is directly proportional to the ratio of labeled to unlabeled GPL in the IM pool. As the bacteria continue to grow in ^{13}C acetate, the ratio of labeled to unlabeled GPL in the IM will gradually increase as new GPL are synthesized and inserted in the IM. As such, the likelihood of transporting labeled GPL to the OM will also increase. A comparison of the ratios of labeled to unlabeled GPL in the IM and OM will thus reflect the efficiency of transport between the membranes, and analysis of transport in wild type *A. baumannii* will establish reference for transport efficiency with which to compare our mutants. Additionally, OM phospholipases, some of which may be activated upon membrane damage (31), will not distinguish between labeled and unlabeled GPL and therefore will not affect the ratio of labeled to unlabeled GPL obtained from this assay.

Membrane separation and analysis of wild type *A. baumannii* revealed near-identical rates-of-change between the two membranes in ratios of ^{13}C-labeled to unlabeled GPLs, indicating that newly synthesized GPLs are transported and inserted into the OM at a rate equivalent to their rate of synthesis and assembly within the IM. Furthermore, the ratios of

labeled to unlabeled GPLs were nearly equal in the IM compared to the OM at the time points evaluated indicating that GPL transport likely occurs rapidly, consistent with earlier pulse-chase experiments performed in *E. coli* that estimate the half-life of translocation of various GPLs at between 0.5 and 2.8 min (32). By contrast, mutants in the Mla system accumulate newly synthesized GPLs in their IM at a greater rate than occurs in the OM as evidenced by the increasing disparity in the ratio of labeled to unlabeled GPLs between the IM and OM over time (Figure 5A). The discrepancy in ratios of labeled to unlabeled GPLs between the IM and OM of Δ*mlaF* is apparent for PG and PE of varying acyl chain lengths corresponding to the most naturally abundant species C16:0/C16:0, C18:1/C18:1, or C16:0/C18:1 (Supplemental File 2). Further, the effects of $MlaF^{K55L}$ expression on GPL trafficking were similar to what was observed in the Δ*mlaF* strain (Figure 5B). Therefore, ATP hydrolysis by MlaF appears to be a requirement for extraction of these GPLs from the IM of *A. baumannii* for subsequent transport to the OM.

To better characterize the role of the periplasmic substrate binding component MlaC, we performed similar stable isotope pulse experiments to observe the flow of newly synthesized GPLs in the Δ*mlaC* strains. Stable isotope experiments on Δ*mlaC* mutants reveal IM accumulation of newly synthesized GPLs similar to the result in Δ*mlaF* mutants (Figure 5 – figure supplement 2A), indicating that in the absence of the periplasmic component GPLs are not efficiently removed from the IM by the remainder of the Mla system. We also sought to characterize the potential role of the putative OM-lipoprotein MlaA, which has been implicated as a component of the Mla system in *E. coli*. A chromosomal deletion strain of *mlaA* was created by allelic exchange, and complemented by expression of MlaA from a pMMB67EH-Kan plasmid. The results of the stable isotope pulse experiments in the Δ*mlaA* strain revealed results consistent with those obtained from Δ*mlaC* and Δ*mlaF*, in which the ratio of labeled to unlabeled GPL is consistently higher in the inner membrane than the outer membrane after one hour of exposure to ^{13}C-acetate (Figure 5 – figure supplement 2B and 2C). These results are consistent with a model in which the IM-localized ABC transporter complex MlaBDEF first transfers GPLs to the periplasmic binding protein MlaC, which then transports GPL to the OM, whereupon MlaA facilitates GPL insertion into the OM.

DISCUSSION

We performed a screen to identify *A. baumannii* proteins that are essential for its OM barrier that led to the identification of an ABC transport system whose ATPase activity maintains OM barrier function. IM and periplasmic components of this system can be purified, bind GPLs, and assemble into a defined protein complex with significant symmetry, indicating that this system could function to transport GPLs from the IM to the OM. Consistent with the possibility that Mla functions as an anterograde transporter, the OM of mutants show an overall reduction of GPL along with an excess accumulation of newly synthesized GPL on the IM. Therefore, these results lead us to propose that the function of the *A. baumannii* Mla system is the trafficking of GPL from the IM, across the periplasm, for delivery to the outer membrane (Figure 6). According to this model, ATP hydrolysis by MlaF provides the initial energy to extract GPL from the IM, while the substrate binding components MlaD and MlaC take up lipids for delivery to the OM. It has been observed by van Meer and colleagues that complete extraction of GPLs from the membrane bilayer requires a Gibbs free energy of ~100 kJ/mol (33, 34), whereas ATP contains just 30 kJ/mol of energy. To account for the energy difference, a hydrophobic acceptor molecule is proposed to allow the lipids to fully dissociate from the rest of the ABC transporter and facilitate complete removal from the bilayer. The GPL-binding component, MlaD, contains an IM spanning domain and is shown here, and in orthologous systems, to be in complex with the MlaE and MlaF proteins within the IM (20, 35). The close association of MlaD with the outer leaflet of the IM may allow it to extract lipids from the IM by hydrophobic interaction with the acyl chains after ATP hydrolysis by MlaF. Subsequent trafficking across the periplasm then involves the periplasmic GPL binding protein MlaC, which likely accepts GPL from MlaD and then carries them to the OM. We note however the observed effect of *mlaC* deletion on GPL accumulation in the IM, while statistically significant for most of the analyzed diacyl-glycerophospholipids, appears to be less than that of deletion of the ATPase component (Figure 5C), suggesting that while MlaC may participate in transfer to the OM, there may be redundant mechanisms by which the IM complex can transport or remove IM GPL in the absence of MlaC. While the precise mechanism of GPL insertion into the OM is not yet known, work performed on the *E.coli* Mla system has shown that MlaC interacts with both the IM MlaFEDB complex, as well as with the putative OM lipoprotein MlaA, and our results support a role for MlaA in the function of the overall Mla system and delivery of GPL to the OM.

In this work, we designed a method to monitor lipid transport between Gram-negative bacterial membranes using stable ^{13}C isotope labeling. We considered the possibility of loss of GPL from the outer membrane due to outer membrane vesicle formation or more likely, by the possible increased activation of outer membrane phospholipases. Both would have the effect of removing GPL from the outer membrane and would result in lower GPL levels in the outer membrane of *mla* mutants. Neither of these mechanisms would operate specifically on either labeled or unlabeled lipids. We understood the decrease in outer membrane GPL to be insufficient evidence of an anterograde transport function for *mla,* and for this reason we developed the stable isotope assay to control for these possibilities. The stable isotope assay gives insight into whether these results are due simply to mislocalization or degradation of outer membrane GPL, or if they can in fact be attributed to deficient anterograde GPL transport. This is because the peak intensity of each newly synthesized, C^{13}-labeled GPL is normalized to the corresponding unlabeled version of that GPL species with each sample injected into the LC-MS/MS. The result is a ratio of labeled to unlabeled GPL for every membrane sample. With C^{13}-acetate as the sole carbon source, we observe a gradual increase in the ratio of labeled GPL relative to unlabeled GPL over time. In wild type bacteria, these ratios for the inner and outer membranes track closely over time, which indicates that under these conditions GPL transport from the inner to the outer membrane occurs quite rapidly. In *mla* mutants the ratio is both higher and typically increases at a greater rate in the inner membrane. Phospholipases and budding outer membrane vesicles will not distinguish between labeled and unlabeled GPL species, and so will not impact the ratios obtained with this assay.

Our results using this assay are consistent with the Mla system functioning as an anterograde GPL transporter, however they do not exclude the possibility of a dual role for Mla components in the maintenance of OM lipid asymmetry. Previous work performed on the orthologous Mla system in *E.coli* has been interpreted to suggest that the function of the system is to remove GPL from the outer leaflet of the OM for retrograde transport back into the cytoplasm based on the observation that *E.coli mla* mutants likely contain GPLs on the outer leaflet of the OM. (12, 36). This proposed function was inferred from the observation that gene deletions resulted in an increased activation of the OM-phospholipase enzymes PagP and OMPLA, suggesting an increased amount of GPL in the outer leaflet of the OM (12). The interpretation of retrograde transport function was also based on the existence of an orthologous

system in plant chloroplasts that transports lipids from the endoplasmic reticulum (ER) into the organelle. Many plants require this retrograde transport function because certain lipids in the chloroplast thylakoid membrane derive from GPL originating in the ER (37). However, since Gram-negative bacteria synthesize GPL within the IM, retrograde transport of GPL would only be necessary for the recycling of GPL mislocalized to the OM outer leaflet. Although this is a reasonable inference based on data available at the time, we would point out that the directionality of transport by the *E. coli* Mla system had not been thoroughly probed experimentally using membrane analysis or with a functional assay of the type performed here. It is conceivable that the import function of the orthologous chloroplast TGD system is a result of adaptation to the intracellular environment, the system in this case having evolved to aid in the transfer of GPL from the nearby ER to the chloroplast. Furthermore, while it is possible that the Mla system in *E. coli* serves a different primary function than in *A. baumannii,* we demonstrate here that both complexes possess a similar architecture, pointing to a conserved function. The outer membrane defect phenotypes observed in *E. coli mla* mutants might also be explained by a disruption of OM structure stemming from decreased concentrations of OM GPL, leading to activation of the PagP enzyme. It is well established that for *E. coli,* GPL displacement to the OM outer leaflet and subsequent activation of these enzymes reflects OM instability and can be achieved by chemical disruption of the bilayer (27-29). It may be the case that the OM of *E. coli mla* mutants contain GPL in the outer leaflet, but the possibility remains that OM GPL can flip into the outer leaflet under conditions of OM damage resulting from an imbalance of LPS-to-GPL ratios, along with perhaps the corresponding disruption of OM proteins. However, final determination of the directionality of GPL transport by the Mla system in *E.coli* and other organisms will require intermembrane transport studies similar to what has been done here for *A. baumannii,* along with studies similar to those performed for the Lpt LPS transport system for which molecular transfer of LPS from molecule to molecule of the Lpt system is functionally defined.

Following the introduction of the retrograde transport model for Mla function into the existing literature, a number of studies have examined the phenotypic effects of Mla disruption in various organisms. In a recent study in PNAS, Powers and Trent first obtained *A. baumannii* deficient in lipooligosaccharide (LOS) by selection in the presence of polymyxin B (38). They then performed an evolution experiment, passaging the strains in cultures containing polymyxin

B over 120 generations, at which point they observed significantly improved growth in the populations. These evolved populations were also observed to have increased resistance to antibiotics including vancomycin, bacitracin, and daptomycin, and to appear more morphologically consistent relative to the unevolved strains when observed microscopically. Whole genome sequencing of the evolved strains revealed mutations in *mla* genes in seven of the 10 evolved populations. They also observed frequent disruptions in *pldA*, as well as in other envelope genes. To further study these effects, they then introduced clean deletions of *mlaE* and *pldA* to ATCC 19606, and selected for LOS-deficient bacteria by plating on polymyxin B. These double mutants demonstrated improved growth and resistance to antibiotics but continued to display altered cellular morphology. The authors present their data as evidence in support of Mla as a retrograde transport system, and assume that a lack of removal of GPL from the outer leaflet is promoting the OM barrier. We would point out that lacking in their data is examination of the membrane glycerophospholipid (GPL) profile in their LOS-deficient mutants. It is assumed by the authors that *mla* and *pldA* mutations have the effect of stabilizing a symmetric outer membrane produced in the absence of LOS by allowing GPL to fill in the outer leaflet, resulting in improved growth and antibiotic resistance. Given that the data suggests that Mla and PldA are selected against when LOS is absent, examination of the outer membrane GPL content might have supported the authors' conclusions if it revealed an increase in GPL in *mla* and *pldA* mutants. Absent such data, it is not obvious to us that the authors have sufficiently ruled out alternative explanations for their observed phenomena. For example, we would question the mechanisms regulating the homeostasis of both the inner and outer membranes and the entire periplasmic space in the absence of LOS. The authors acknowledge earlier work that observed an increase in expression of *mla* genes upon initial loss of LOS in 19606 (39, 40). Genes in the *mla* pathway were shown to have an up to 7.5-fold increase in gene expression upon loss of LOS. Powers and Trent assert that the function of Mla is deleterious in the absence of LOS, but perhaps what is deleterious is the profound upregulation of *mla* expression in the absence of LOS, combined with an active PldA. If Mla is an anterograde transporter, we can imagine this might create a situation in which GPL are rapidly removed from the inner membrane and then degraded in the outer membrane in excess of what the cell can support and limiting both of these processes together simply allows the cell to achieve a new homeostasis. Understanding of the myriad processes regulating bacterial outer membrane assembly and integrity remains limited

even when LOS is present, and so interpreting results such as these as providing direct evidence of function may exceed the limits of the data.

The gene for MlaA, the proposed OM component, is at a different chromosomal location from the remainder of the *mla* operon. Recent structural studies on MlaA have revealed that MlaA forms a ring-shaped structure localized the inner leaflet of the OM, and have shown it to form stable complexes with the outer membrane proteins OmpF and OmpC (41). The proposed structure of MlaA in the OM supports the argument that MlaA is involved in removal of GPL from the outer leaflet, and it is suggested that GPL from the outer leaflet travel through a pore in MlaA where they are received by MlaC, yet our data reveals that *A. baumannii* Δ*mlaA* mutants are defective in delivery of GPL from the IM to the OM. These data can be reconciled by a model in which MlaA functions both to remove mislocalized GPL from the outer leaflet of the OM, and additionally serves to facilitate delivery of GPL to the OM by MlaC, perhaps by enabling MlaC localization to the surface of the inner leaflet. By this model, mutations in MlaA will be phenotypically similar to mutations in other components of the Mla system, and we would expect to observe a decreased rate of anterograde GPL transport. We would here point out that while previous work has implicated the Mla system in the maintenance of OM lipid asymmetry through observation of increased activity of PagP, the role of the MlaFEDB complex and MlaC in retrograde GPL transport has previously only been inferred from homology to the chloroplast TGD system. It is established that cellular mechanisms exist in Gram-negative bacteria to resist stressful conditions that lead to OM disruption. For example, OM phospholipase enzymes, such as PldA, are activated under conditions of membrane stress to digest GPL in the outer leaflet of the OM, as high levels of GPL in the outer leaflet destabilize the OM barrier function. The model of retrograde GPL transport by the Mla system proposes that growing cells expend cellular energy in the form of ATP in order to transport undigested GPL from the OM, across the periplasm, and back into the IM, at which point some of those same molecules will be transported back to the OM by an unknown mechanism. However, the available data points most clearly to a model of anterograde GPL transport by MlaFEDB and MlaC, facilitated in some way by MlaA.

The first three genes of the *mla* operon – comprising an ATPase, permease, and substrate-binding components of the ABC transporter complex – are conserved in *Mycobacteria spp, Actinobacteria,* and chloroplasts, while the entire five-gene operon appears to be conserved in

Gram-negative bacteria (42). Given the conservation of the system across Gram-negative species, our results may shed light on a generalized mechanism contributing to OM biogenesis. Additionally, we have here demonstrated that the function of this ABC transport system is crucial for maintaining the integrity of the *A. baumannii* OM. The fact that *mla* mutations are tolerated, and that levels of OM GPL are reduced but not abolished, suggests the intriguing possibility of additional undiscovered mechanisms of GPL delivery to the OM. Also of interest is the potential role of the increased exopolysaccharide observed upon disruption of the Mla system. It is possible this exopolysaccharide plays a partially compensatory role in *A. baumannii* resulting from decreased OM GPL, given that recent work has shown that *A. baumannii* exopolysaccharides can contribute to antibiotic resistance, likely through improved barrier function (43).

The progression towards a more complete understanding of intermembrane GPL transport and OM barrier function should ultimately have relevance in the development of novel drug targets to undermine emerging antibiotic resistance in Gram-negative pathogens. The emergence of antibiotic resistant Gram-negative bacteria for which few or no antibiotics are available therapeutically is an important medical concern. This issue is typified by current isolates of *A. baumannii* that can only be treated with relatively toxic colistin antibiotics. This has led many individuals and agencies to propose the development of single agent antimicrobials which could be used for organisms such as *A. baumannii* and *P. aeruginosa* that have significant antibiotic resistance. Therefore, work furthering the understanding of the OM barrier could lead to the development of drugs which target the barrier and allow the therapeutic use of many current antibiotics.

MATERIALS AND METHODS

Key Resources Table

Reagent type (species) or resource	Designation	Source or reference	Identifiers	Additional information
gene (Acinetobacter baumannii)	*mlaC*	NA	Genbank Accession: AKA30172.1	
gene (A. baumannii)	*mlaF*	NA	Genbank Accession: AKA30169.1	
gene (A. baumannii)	*mlaE*	NA	Genbank Accession: AKA30170.1	
gene (A. baumannii)	*mlaD*	NA	Genbank Accession: AKA30171.1	

gene (A. baumannii)	*mlaB*	NA	Genbank Accession: AKA30173.1	
gene (A. baumannii)	*mlaA*	NA	Genbank Accession: AKA32955.1	
gene (A. baumannii)	*phoU*	NA	Genbank Accession: AKA33305.1	
strain, strain background (A. baumannii)	*Acinetobacter baumannii* ATCC 17978	Reference: PIECHAUD, D., M. PIECHAUD, AND L. SECOND. 1951. Etude de 26 souches de Moraxella iwoffi. Ann. Inst. Pasteur 80:97-99; PMCID: PMC251972. Source: ATCC	GenBank ACCESSION: CP000521	
genetic reagent (A. baumannii)	ATCC 17978 ΔphoU	This paper		Chromosomal deletion in ATCC 17978 by allelic exchange using pEX2tetRA vector
genetic reagent (A. baumannii)	Δ*mlaF*	This paper		Chromosomal deletion in ATCC 17978 by allelic exchange using pEX2tetRA vector
genetic reagent (A. baumannii)	Δ*mlaC*	This paper		Chromosomal deletion in ATCC 17978 by allelic exchange using pEX2tetRA vector
genetic reagent (A. baumannii)	Δ*mlaA*	This paper		Chromosomal deletion in ATCC 17978 by allelic exchange using pEX2tetRA vector
antibody	anti-OmpA (rabbit polyclonal)	This paper		Made to purified OmpA by GenScript Biotech Corp (1:1000)
recombinant DNA reagent	pMarKT (plasmid)	This paper		Progenitors: C9 Himar (PCR), TetRA from Tn10 (PCR), pACYC184, pBT20.
recombinant DNA reagent	pEX2tetRA (plasmid)	This paper		Progenitors: tetRA (PCR), pEXG2
recombinant DNA reagent	pMMBkan (plasmid)	This paper		Kanamycin resistance marker inserted at DraI site of pMMB67EH
recombinant DNA reagent	pMMBkan:MlaF (plasmid)	This paper		pMMBKan expressing *mlaF*
recombinant DNA reagent	pMMBkan:MlaF^{K55L} (plasmid)	This paper		pMMBKan expressing Walker box mutant of *mlaF*
recombinant DNA reagent	pET28a:MlaFEDCB-His (plasmid)	This paper		pET28a expressing MlaFEDCB with C-terminal HISX6 tag on MlaB.
recombinant DNA reagent	pET15b-mlaC-SD-His (plasmid)	This paper		pET15b expression vector containing MlaC soluble domain with C-terminal HisX6 tag.
recombinant DNA reagent	pET15b-mlaD-SD-His (plasmid)	This paper		pET15b expression vector containing MlaD soluble domain with C-terminal HisX6 tag.
chemical compound, drug	2-13C acetate	Cambridge Isotope Laboratories, Inc.		
chemical compound, drug	BCIP-Toluidine (XP)	Gold Biotechnology	B-500-10	

chemical compound, drug	N-Phenyl-1-naphthylamine (NPN)	Sigma Aldrich	104043-500G	
chemical compound, drug	NADH	Sigma Aldrich	606-68-8	
chemical compound, drug	CCCP (Carbonyl cyanide 3-chlorophenylhydrazone)	Sigma-Aldrich	C2759-1G	
software, algorithm	MotionCorr2	Zheng et al, 2016, Nature Methods. PMID: 28250466		Dr. Agard Lab, University of CA San Francisco
software, algorithm	CTFFIND4	Rohou & Grigorieff, 2015, J Struct Biol. PMID: 26278980		Dr. Grigorieff Lab, University of MA Medical Center
software, algorithm	Appion	Lander et al, 2009, J Struct Biol. PMID: 19263523		Dr. Carragher Lab, The Scripps Research Institute
software, algorithm	Relion 2	Scheres, 2012, J Mol Biol. PMID: 22100448		Dr. Scheres Lab, MRC Lab of Molecular Biology
software, algorithm	EMAN2	Tang et al, 2007, J Struct Biol. PMID: 16859925		Dr. Ludtke Lab, Blue Mountain College
software, algorithm	Chimera	Pettersen et al, 2004, J Comput Chem. PMID: 15264254		UCSF Resource for Biocomputing, Visualization, and Informatics
software, algorithm	Modeller	Webb & Sali, 2016, Current Protocols in Bioinformatics. PMID: 27322406		Dr. Sali Lab, University of CA San Francisco
software, algorithm	Rosetta	DiMaio et al, 2011, PLoS One. PMID: 21731614		Dr. Baker Lab, University of WA

Bacterial strains:

Transposon mutagenesis and subsequent chromosomal deletions of *mla* genes were performed in *Acinetobacter baumannii* ATCC 17978.

A Mariner-based transposon vector for use in *Acinetobacter baumannii:*

To perform transposon mutagenesis a Mariner-based transposon vector was designed for use in *Acinetobacter baumannii* ATCC 17978. The new transposon vector, derived from pBT20, termed pMarKT, contains an outward facing pTac promotor as well as a selectable kanamycin resistance marker followed by an omega terminator within the Mariner arm sites **(44)**. The plasmid backbone contains the Mariner transposase gene C9 Himar, a *tetRA* resistance marker from Tn10, a p15A origin from pACYC184, and an oriT site for mobilization. The plasmid was constructed by PCR of select fragments followed by restriction digest and ligation of the cleaved

ends. The new transposon vector was confirmed by restriction digest and partial sequencing.

Transposon mutagenesis:

Initial mutagenesis revealed that many hits occurred in the high affinity phosphate uptake transcriptional repressor *phoU* (A1S_0256). Subsequent rounds of mutagenesis were conducted on an ATCC 17978 *phoU* chromosomal deletion strain, and plated on high phosphate media to reduce the background level of cleavage of the chromogenic substrate. Chromosomal deletions were performed by allelic exchange using a pEX2tetRA vector, which was created by insertion of the *tetRA* tetracycline resistance marker from Tn10 into the pEXG2 plasmid **(45)**. Roughly 1000bp regions upstream and downstream of the genes of interest were amplified for homologous recombination with the ATCC 17978 chromosome. Sucrose was used to counter-select against cells retaining the pEX2tetRA backbone, and deletions were confirmed by PCR. Complementation of deletions was accomplished by repairing the original deletion in the chromosome, again using the pEX system and allelic exchange.

Donor *E. coli* containing the pMarKT transposon vector were suspended in LB broth to an OD_{600} of 40 and mixed with an equal volume of the recipient *A. baumannii* suspended to OD_{600} of 20. 50 µL aliquots of this mixture were then plated in spots on a dried LB agar plate and incubated for 2 h at 37 °C **(44)**. Each 50 µL spot resulted in about 80,000 colonies of *A. baumannii* containing Mariner transposon insertions. The mutants were plated on LB agar containing 1X M63 salts, 50 µg/mL kanamycin, 30 µg/mL chloramphenicol, and 40 µg/mL XP substrate. Plates were incubated for at least 36 h at 30 °C to allow for the appearance of the blue color from cleavage of the XP substrate. Sequencing of the transposon insertions was adapted from the method described in Chun et. al. **(46)**, including semi-arbitrary two-step PCR amplification of transposon regions followed by sequencing.

Ethidium bromide uptake assay:

Bacteria were grown in 5 mL LB cultures to mid-log OD600 (0.3-0.6), then spun down and normalized in PBS to OD600 0.2. Prior to measurement, CCCP was added at 200 µM to inhibit the activity of efflux pumps. Ethidium bromide was added immediately prior to measurement to final concentration of 1.2 µM in 200 µL total reaction volume. Permeability was assessed using a PerkinElmer EnVision 2104 Multilabel Reader using a 531 nm excitation filter, 590 nm emission

filter, and a 560 nm dichroic mirror. Readings were taken every 15 s for 30 min with samples assessed in triplicate in a Greiner bio-one 96-well flat bottom black plate.

MIC measurements:

MICs were determined in 96-well microtiter plates using a standard two-fold broth dilution method of antibiotics in LB broth. The wells were inoculated with 10^4 bacteria per well, to a final well volume of 100 μL, and plates were incubated at 37 °C with shaking unless stated otherwise. Experiments were performed thrice using two technical replicates per experiment. MICs were interpreted as the lowest antibiotic concentration for which the average OD_{600} across replicates was less than 50% of the average OD_{600} measurement without antibiotic.

Crystal violet assay for exopolysaccharide production:

Strains were inoculated to OD_{600} 0.05 and grown overnight at 37 °C in 2 mL LB broth with shaking in glass tubes. The next day, liquid was carefully decanted and the tubes left to dry for 2 h at 37 °C. Pellicles were stained with the addition of 0.1% crystal violet, then gently washed three times in dH_2O. Crystal violet was solubilized in a 80:20 solution of ethanol:acetone and read at 590 nm. P values were determined from a Student's t-test over three biological replicates per sample.

MlaFEDB protein expression and purification:

The *mlaFEDCB* operon from the genome of *A. baumannii* ATCC 17978 was subcloned into the pET-28a vector (Novagen, US) with a hexahistidine (-6HIS) tag fused at the C-terminus of the MlaB protein. The nucleotide sequence of the operon was confirmed using DNA sequencing. The plasmid was transformed into *E. coli* RosettaBlue strain. Cells were grown at 37 °C in LB medium until the cell density reached an OD600 of 1.0. The temperature was then reduced to 16 °C before induction with 1 mM isopropyl β-D-thiogalactoside (IPTG). After growth at 16 °C for 18 h, cells were harvested by using centrifugation at 4,200 g. Cells were resuspended in ice-cold buffer A (20 mM Tris-HCl (pH 8.0), 150 mM NaCl, 5% (v/v) glycerol) and subjected to three runs of homogenization at 10,000–15,000 psi using Avestin EmulsiFlex-C3 high pressure homogenizer (Avestin, Ottawa, Ontario, Canada). The homogenate was centrifuged at 17,000 g for 10 min at 4 °C, and then the supernatant was ultra-centrifuged at 100,000 g for 60 min. The

membrane fraction was resuspended in buffer A supplemented with 1% (w/v) dodecyl-β-d-maltopyranoside (DDM) and was slowly stirred for 1 h at 4 °C. After another ultra-centrifugation at 100,000 g for 30 min, the supernatant was collected and loaded on 2 ml of Ni^{2+}-nitrilotriacetate affinity resin (Ni-NTA from Qiagen, Germany) pre-equilibrated with buffer A supplemented with 5 mM imidazole and 0.025% (w/v) DDM. After incubating for 1 h, the resin was washed with 50 ml buffer A supplemented with 20 mM imidazole and 0.025% (w/v) DDM. The protein sample was eluted with 10 ml elution buffer containing buffer A, 300 mM imidazole, and 0.025% (w/v) DDM, and was concentrated to 0.5 ml. The concentrated protein sample was then loaded onto a Superdex-200 column (10/30, GE Healthcare, US) pre-equilibrated with 20 mM Hepes (pH 7.0) 150 mM Nacl 0.025% DDM. Peak fractions were collected and the pooled protein sample was concentrated to 1 mg/ml.

Cryo-EM sample preparation, data acquisition and image processing:

Purified Mla complex at ~1 mg/ml was applied to glow-discharged holey grids, blotted for 6 s, and plunged in liquid ethane using a Vitrobot (FEI). Images were acquired on a FEI Tecnai G2 F20 200 kV Cryo-TEM equipped with a Gatan K-2 Summit Direct Electron Detector camera with a pixel size of 1.26 Å/pixel. 500 micrographs were collected using Leginon (47) spanning a defocus range of -1 to -2 µm.

Movie frames were aligned with MotionCorr2 (48) and the defocus parameters were estimated with CTFFIND4 (49). 333 high-quality micrographs were selected by manual inspection, from which ~55,000 particles were picked with DOG in Appion (50). Particle stacks were generated in Appion using a box size of 200 pixels. Several successive rounds of 2D and 3D classification were performed in Relion 2 (51, 52) using an initial model generated by Common Lines in EMAN2 (53) leading to a final stack of ~ 14,000 particles for 3D structure refinement in Relion.

Structure modeling and docking in the EM density:

The structures of MlaB and MlaF were modeled using the threading server Phyre (54) based on the structures of the anti-sigma factor antagonist tm1081 (PDB ID 3F43, 18% sequence identity to MlaB) and the ABC ATPase ABC2 (PDB ID 1OXT, 36% sequence identity to MlaF) respectively. Two copies of each structural model were positioned in their putative location

within the EM map using Chimera (55) and their position was optimised using the Fit to EM map option. The abMlaD and abMlaE structures were modelled on ecMlaD and ecMlaE structural models deposited in the Gremelin database (21), using Modeller. For abMlaD, the N-terminal TM helix and the insert region were modelled ab initio using the Rosetta suite (56) and positioned in their putative localisation in Chimera. The MlaD hexamer, as well as the MlaE dimer, were modelled with Rosetta using a EM-guided symmetry modelling approach described previously (22). The final model was refined with Rosetta.

Membrane Isolation and Separation

Cells were resuspended in 20 mL of 0.5 M sucrose, 10 mM Tris pH 7.8, 75 µg freshly prepared lysozyme (Roche 10837059001), and 20 mL of 0.5 mM EDTA, and kept on ice with gentle stirring for 20 min. Samples were homogenized (Avestin EmulsiFlex-C3) and spun down at 17,000 g for 10 min to removed un-lysed cells prior to ultracentrifugation. Membranes were spun down using a Ti45 Beckman rotor at 100,000 g for 1 h and then added to the top of a sucrose gradient. IM and OM were separated by 18-hour ultracentrifugation using a SW-41 rotor in a Beckman Coulter Optima L90X ultracentrifuge. Spheroplast formation and sucrose gradient separation of IM and OM was adapted from a method by Osborn et. al (57) by use of a defined 73%-53%-20% sucrose gradient as described in Dalebroux et. al. (58). Our sucrose gradients contain three distinct concentrations of sucrose, and inner and outer membranes separate into distinct bands that are collected individually (Figure 5 – figure supplement 3F). To limit any potential mixing of the membranes, the inner membrane is collected from the top of the tube while the outer membrane is collected by puncturing the bottom of the tube and allowing the bottom band to be collected. The purity of membrane separation by this method was confirmed by NADH assay and by Western blotting for the *A. baumannii* OM-localized OmpA protein, with 10 µg of total protein loaded into each lane as measured by Bradford protein assay (Figure 5 – figure supplement 3).

GPL extraction and TLC:

GPLs from isolated membranes were extracted using a 0.8:1:2 ratio of water : chloroform : methanol as per the method of Bligh and Dyer (59). Two-dimensional TLC was performed using silica gel 60 plates and immersion in Solvent System A (60:25:4 $CHCl_3$:CH_3OH:H_2O), followed by Solvent System B (80:12:15:4 $CHCl_3$:CH_3OH:CH_3COOH:H_2O) in the orthogonal direction.

MlaC and MlaD protein purification and GPL extraction:

Primers were designed to amplify the *mlaC* gene of ATCC 17978, excluding the signal sequence for export from the cytoplasm, and the periplasmic domain of *mlaD* of ATCC 17978, excluding the membrane-spanning domain. These fragments were cloned into pET29b and expressed with a carboxy-terminal hexahistidine (-6HIS) tag in BL21 *E. coli* with 2 h induction. Cells were pelleted and resuspended in Tris-buffered saline containing 10% glycerol (TBSG) and protease inhibitor cocktail (Roche, Complete EDTA-free). Cells were lysed by homogenization (Avestin) and ultracentrifuged at 100,000 g for 1 h to spin down membranes. The supernatants were then applied to a 5 mL-HiTrap(TM) Chelating HP Ni-affinity column pre-loaded with 0.1 M $NiSO_4$ and equilibrated with TBSG. The proteins were eluted from the column using FPLC (Akta) by applying a stepwise gradient of 25 mM, 50 mM, and finally 300 mM imidazole for protein elution. Elution was monitored by UV-absorption at 280 nm. The MlaC- and MlaD-containing fractions were then further purified by injecting into a HiLoad 120 ml-6/600 Superdex(TM) 200 preparative grade size-exclusion column equilibrated in TBSG using a flow rate of 1 mL/min. The purity of the collected protein fractions was confirmed by SDS polyacrylamide gel electrophoresis. Proteins were diluted to 2 mg/mL and dialyzed overnight in 1 L TBSG at 4 °C with stirring. GPLs were extracted from 1 mg each of purified proteins MlaC and MlaD by the method of Bligh and Dyer and analyzed by LC-MS/MS as previously described.

LC-MS/MS:

Retention of PG, CL, PE, and Lyso-CL was achieved at a flow rate of 0.3 mL/min using mobile phase A [$CHCl_3$/CH_3OH/NH_4OH (800:195:5 v/v/v)] and mobile phase B [$CHCl_3$/CH_3OH/NH_4OH (600:340:5 v/v/v)]. The chromatography method used is a three-step gradient as described in the SI Materials and Methods of Dalebroux et al. (26). The samples were run on an Agilent Zorbax Rx-SIL silica column (2.1x100mm, 1.8-Micron) using an Agilent HPLC autosampler. Mass spectrometry was performed using an AB Sciex API4000 Qtrap with multiple reaction monitoring (MRM). The identities of the major GPLs present in the *A. baumannii* membrane were predicted by parent ion scans.

Stable isotope assay development:

The Q1/Q3 transitions of glycerolphospholipids from cells grown in 2-^{13}C acetate were determined using a Thermo Orbitrap LTQ. The integrated peak areas of both ^{13}C-labeled and unlabeled GPLs from the AB Sciex API4000 Qtrap were used to calculate the ion-current ratios for each GPL species. The ratio of labeled GPL for each unique species can be calculated based on the following equation:

$$R_{lab} = R_i - R_b \quad \textbf{(60)}$$

Where R_i is the ion-current ratio of labeled GPL to unlabeled GPL within the sample and R_b is the ion-current ratio of samples before the administration of the tracer, ^{13}C-acetate, and represents the natural background abundance of the stable isotope species within the bacterial membrane. R_{lab} approximates the molar ratio of labeled species to unlabeled species (n_{lab}/n_{un}) according to the equation $(n_{lab}/n_{un}) = [R_i-R_b]/k$, where k is the molar response factor of the instrument and is ideally equal to unity **(60)**.

To demonstrate that OM phospholipases will not distinguish between labeled and unlabeled GPL and therefore will not affect the ratio of labeled to unlabeled GPL obtained from this assay, we compared ratios of labeled and unlabeled GPL from wild type *A. baumannii* and deletion mutants in *pldA*. Bacteria were grown carrying either the empty pMMB::*kan* vector, or expressing the Walker box mutant MlaF^{K55L}. Accumulation of newly synthesized GPL was observed in those strains expressing MlaF^{K55L} when compared to the vector control, across various species of GPL. Of strains expressing the vector control, on average 51.84% ± 1.07% and 52.07% ± 1.23% of newly synthesized PG C16:0/18:1 appeared on the inner membrane of wild type and Δ*pldA*, respectively, after one hour incubation with ^{13}C acetate, while 66.33% ± 1.23% and 62.60% ± 1.70% of newly synthesized PG C16:0/18:1 accumulated at the inner membranes of wild type and Δ*pldA* expressing MlaF^{K55L}. In vector controls strains, 48.53% ± 1.37% and 51.01% ± 0.55% of newly synthesized PG C16:0/16:0 appeared on the inner membrane of wild type and Δ*pldA*, respectively, after one hour incubation with ^{13}C acetate, while 62.98% ± 1.01% and 60.41% ± 1.25% of newly synthesized PG C16:0/16:0 accumulated at the inner membranes of wild type and Δ*pldA* expressing MlaF^{K55L}. In vector controls strains, 50.17% ± 1.31% and 50.49% ± 1.15% of newly synthesized PE C16:0/18:1 appeared on the

719 inner membrane of wild type and Δ*pldA*, respectively, while 60.14% ± 0.93% and 62.06% ±
720 1.07% of newly synthesized PE C16:0/18:1 accumulated at the inner membranes of wild type
721 and Δ*pldA* expressing $MlaF^{K55L}$.
722
723 **Stable isotope GPL analysis and culture conditions:**
724 Cultures of *A. baumannii* ATCC 17978 were grown in M63 media containing 5 mM sodium
725 acetate and 4 mM $MgCl_2$ to OD600 0.4, then washed and resuspended in media containing 5 mM
726 2-^{13}C sodium acetate (Cat. No. CLM-381-0, Cambridge Isotope Laboratories, Inc.). Membrane
727 fractions were isolated from both wild type and *mla* mutant *A. baumannii* at simultaneous time
728 points, and GPL were extracted and assessed using previously established LC-MS/MS methods
729 with additional MRM values to account for the increased m/z ratios of ^{13}C-labeled GPL. MRMs
730 were selected to account for PG and PE having acyl chains of either C16:0/16:0, C16:0/18:1, and
731 C18:1/18:1 as these were determined by total ion scan MS to be the predominant species of PG
732 and PE GPL. Pulse experiments were performed at least twice for each mutant.
733
734 **Acknowledgements**
735 We thank Dale Whittington and Dr. Scott Edgar at the Mass Spectrometry Center, Department of
736 Medicinal Chemistry, University of Washington for technical help with MS analysis; and Mauna
737 Edrozo for technical help.
738
739 **Author Information**
740 Authors have no competing financial interests. Correspondence and Requests for materials
741 should be addressed to SIM (millersi@uw.edu).
742
743 **Data Availability**
744 The cryo-EM map has been deposited in the Electron Microscopy Data Bank with accession
745 code EMD-0007 (8.7 Å map). The coordinates for the MlaBDEF model have been deposited to
746 PDB, accession number 6IC4.
747
748 **References:**
749 **1. Zhang YM, Rock CO. Membrane lipid homeostasis in bacteria. Nat Rev Microbiol.**
750 **[Research Support, N.I.H., Extramural**
751 **Research Support, Non-U.S. Gov't**
752 **Review]. 2008 Mar;6(3):222-33.**
753 **2. Pelletier MR, Casella LG, Jones JW, Adams MD, Zurawski DV, Hazlett KR, et al.**
754 **Unique structural modifications are present in the lipopolysaccharide from colistin-**

resistant strains of Acinetobacter baumannii. Antimicrob Agents Chemother. [Research Support, N.I.H., Extramural Research Support, Non-U.S. Gov't]. 2013 Oct;57(10):4831-40.

3. Bishop RE. Emerging roles for anionic non-bilayer phospholipids in fortifying the outer membrane permeability barrier. J Bacteriol. [Comment Research Support, Non-U.S. Gov't]. 2014 Sep;196(18):3209-13.

4. Okuda S, Tokuda H. Lipoprotein sorting in bacteria. Annu Rev Microbiol. [Research Support, Non-U.S. Gov't Review]. 2011;65:239-59.

5. Okuda S, Sherman DJ, Silhavy TJ, Ruiz N, Kahne D. Lipopolysaccharide transport and assembly at the outer membrane: the PEZ model. Nat Rev Microbiol. 2016 Jun;14(6):337-45.

6. Chmelnitsky I, Shklyar M, Hermesh O, Navon-Venezia S, Edgar R, Carmeli Y. Unique genes identified in the epidemic extremely drug-resistant KPC-producing Klebsiella pneumoniae sequence type 258. J Antimicrob Chemother. 2012 Oct 4.

7. Abbo A, Navon-Venezia S, Hammer-Muntz O, Krichali T, Siegman-Igra Y, Carmeli Y. Multidrug-resistant Acinetobacter baumannii. Emerg Infect Dis. 2005 Jan;11(1):22-9.

8. Strauch KL, Beckwith J. An Escherichia coli mutation preventing degradation of abnormal periplasmic proteins. Proc Natl Acad Sci U S A. [Research Support, Non-U.S. Gov't Research Support, U.S. Gov't, P.H.S.]. 1988 Mar;85(5):1576-80.

9. Lopes J, Gottfried S, Rothfield L. Leakage of periplasmic enzymes by mutants of Escherichia coli and Salmonella typhimurium: isolation of "periplasmic leaky" mutants. J Bacteriol. 1972 Feb;109(2):520-5.

10. Helander IM, Mattila-Sandholm T. Permeability barrier of the gram-negative bacterial outer membrane with special reference to nisin. Int J Food Microbiol. [Research Support, Non-U.S. Gov't]. 2000 Sep 25;60(2-3):153-61.

11. Murata T, Tseng W, Guina T, Miller SI, Nikaido H. PhoPQ-mediated regulation produces a more robust permeability barrier in the outer membrane of Salmonella enterica serovar typhimurium. J Bacteriol. [Research Support, N.I.H., Extramural]. 2007 Oct;189(20):7213-22.

12. Malinverni JC, Silhavy TJ. An ABC transport system that maintains lipid asymmetry in the gram-negative outer membrane. Proc Natl Acad Sci U S A. [Research Support, N.I.H., Extramural]. 2009 May 12;106(19):8009-14.

13. Nikaido H. Molecular basis of bacterial outer membrane permeability revisited. Microbiol Mol Biol Rev. [Research Support, U.S. Gov't, P.H.S. Review]. 2003 Dec;67(4):593-656.

14. Vaara M. Agents that increase the permeability of the outer membrane. Microbiol Rev. [Research Support, Non-U.S. Gov't Review]. 1992 Sep;56(3):395-411.

15. Walker JE, Saraste M, Runswick MJ, Gay NJ. Distantly related sequences in the alpha- and beta-subunits of ATP synthase, myosin, kinases and other ATP-requiring enzymes and a common nucleotide binding fold. Embo J. [Comparative Study Research Support, Non-U.S. Gov't]. 1982;1(8):945-51.

16. Hanson PI, Whiteheart SW. AAA+ proteins: have engine, will work. Nat Rev Mol Cell Biol. [Review]. 2005 Jul;6(7):519-29.

17. Davidson AL, Sharma S. Mutation of a single MalK subunit severely impairs maltose transport activity in Escherichia coli. J Bacteriol. [Research Support, U.S. Gov't, P.H.S.]. 1997 Sep;179(17):5458-64.
18. Wilkens S. Structure and mechanism of ABC transporters. F1000Prime Rep. [Review]. 2015;7:14.
19. Thong S, Ercan B, Torta F, Fong ZY, Wong HY, Wenk MR, et al. Defining key roles for auxiliary proteins in an ABC transporter that maintains bacterial outer membrane lipid asymmetry. Elife. 2016;5.
20. Ekiert DC, Bhabha G, Isom GL, Greenan G, Ovchinnikov S, Henderson IR, et al. Architectures of Lipid Transport Systems for the Bacterial Outer Membrane. Cell. 2017 Apr 06;169(2):273-85 e17.
21. Ovchinnikov S, Park H, Varghese N, Huang PS, Pavlopoulos GA, Kim DE, et al. Protein structure determination using metagenome sequence data. Science. 2017 Jan 20;355(6322):294-8.
22. Bergeron JR, Worrall LJ, Sgourakis NG, DiMaio F, Pfuetzner RA, Felise HB, et al. A refined model of the prototypical Salmonella SPI-1 T3SS basal body reveals the molecular basis for its assembly. PLoS Pathog. [Research Support, N.I.H., Extramural Research Support, Non-U.S. Gov't]. 2013;9(4):e1003307.
23. Khare D, Oldham ML, Orelle C, Davidson AL, Chen J. Alternating access in maltose transporter mediated by rigid-body rotations. Mol Cell. [Research Support, N.I.H., Extramural
Research Support, Non-U.S. Gov't]. 2009 Feb 27;33(4):528-36.
24. Oldham ML, Chen S, Chen J. Structural basis for substrate specificity in the Escherichia coli maltose transport system. Proc Natl Acad Sci U S A. [Research Support, N.I.H., Extramural
Research Support, Non-U.S. Gov't]. 2013 Nov 05;110(45):18132-7.
25. Huang YM, Miao Y, Munguia J, Lin L, Nizet V, McCammon JA. Molecular dynamic study of MlaC protein in Gram-negative bacteria: conformational flexibility, solvent effect and protein-phospholipid binding. Protein Sci. 2016 Aug;25(8):1430-7.
26. Dalebroux ZD, Matamouros S, Whittington D, Bishop RE, Miller SI. PhoPQ regulates acidic glycerophospholipid content of the Salmonella Typhimurium outer membrane. Proc Natl Acad Sci U S A. [Research Support, N.I.H., Extramural Research Support, Non-U.S. Gov't]. 2014 Feb 4;111(5):1963-8.
27. Jia W, El Zoeiby A, Petruzziello TN, Jayabalasingham B, Seyedirashti S, Bishop RE. Lipid trafficking controls endotoxin acylation in outer membranes of Escherichia coli. J Biol Chem. [Research Support, Non-U.S. Gov't]. 2004 Oct 22;279(43):44966-75.
28. Bishop RE, Gibbons HS, Guina T, Trent MS, Miller SI, Raetz CR. Transfer of palmitate from phospholipids to lipid A in outer membranes of gram-negative bacteria. Embo J. [Comparative Study
Research Support, Non-U.S. Gov't
Research Support, U.S. Gov't, P.H.S.]. 2000 Oct 02;19(19):5071-80.
29. Dekker N. Outer-membrane phospholipase A: known structure, unknown biological function. Mol Microbiol. [Review]. 2000 Feb;35(4):711-7.
30. Kumari S, Beatty CM, Browning DF, Busby SJ, Simel EJ, Hovel-Miner G, et al. Regulation of acetyl coenzyme A synthetase in Escherichia coli. J Bacteriol. [Research Support, U.S. Gov't, Non-P.H.S.]. 2000 Aug;182(15):4173-9.

31. Istivan TS, Coloe PJ. Phospholipase A in Gram-negative bacteria and its role in pathogenesis. Microbiology. [Review]. 2006 May;152(Pt 5):1263-74.
32. Donohue-Rolfe AM, Schaechter M. Translocation of phospholipids from the inner to the outer membrane of Escherichia coli. Proc Natl Acad Sci U S A. [Research Support, U.S. Gov't, P.H.S.]. 1980 Apr;77(4):1867-71.
33. Abreu MS, Moreno MJ, Vaz WL. Kinetics and thermodynamics of association of a phospholipid derivative with lipid bilayers in liquid-disordered and liquid-ordered phases. Biophys J. [Research Support, Non-U.S. Gov't]. 2004 Jul;87(1):353-65.
34. van Meer G, Halter D, Sprong H, Somerharju P, Egmond MR. ABC lipid transporters: extruders, flippases, or flopless activators? FEBS Lett. [Research Support, Non-U.S. Gov't]. 2006 Feb 13;580(4):1171-7.
35. Roston RL, Gao J, Murcha MW, Whelan J, Benning C. TGD1, -2, and -3 proteins involved in lipid trafficking form ATP-binding cassette (ABC) transporter with multiple substrate-binding proteins. J Biol Chem. [Research Support, Non-U.S. Gov't]. 2012 Jun 15;287(25):21406-15.
36. Benning C. A role for lipid trafficking in chloroplast biogenesis. Prog Lipid Res. [Research Support, U.S. Gov't, Non-P.H.S.
Review]. 2008 Sep;47(5):381-9.
37. Hurlock AK, Roston RL, Wang K, Benning C. Lipid trafficking in plant cells. Traffic. [Research Support, Non-U.S. Gov't
Research Support, U.S. Gov't, Non-P.H.S.
Review]. 2014 Sep;15(9):915-32.
38. Powers MJ, Trent MS. Phospholipid retention in the absence of asymmetry strengthens the outer membrane permeability barrier to last-resort antibiotics. Proc Natl Acad Sci U S A. [Research Support, N.I.H., Extramural
Research Support, U.S. Gov't, Non-P.H.S.]. 2018 Sep 4;115(36):E8518-E27.
39. Henry R, Vithanage N, Harrison P, Seemann T, Coutts S, Moffatt JH, et al. Colistin-resistant, lipopolysaccharide-deficient Acinetobacter baumannii responds to lipopolysaccharide loss through increased expression of genes involved in the synthesis and transport of lipoproteins, phospholipids, and poly-beta-1,6-N-acetylglucosamine. Antimicrob Agents Chemother. [Research Support, Non-U.S. Gov't]. 2012 Jan;56(1):59-69.
40. Boll JM, Crofts AA, Peters K, Cattoir V, Vollmer W, Davies BW, et al. A penicillin-binding protein inhibits selection of colistin-resistant, lipooligosaccharide-deficient Acinetobacter baumannii. Proc Natl Acad Sci U S A. [Research Support, N.I.H., Extramural
Research Support, Non-U.S. Gov't]. 2016 Oct 11;113(41):E6228-E37.
41. Abellon-Ruiz J, Kaptan SS, Basle A, Claudi B, Bumann D, Kleinekathofer U, et al. Structural basis for maintenance of bacterial outer membrane lipid asymmetry. Nat Microbiol. 2017 Dec;2(12):1616-23.
42. Casali N, Riley LW. A phylogenomic analysis of the Actinomycetales mce operons. BMC Genomics. [Research Support, N.I.H., Extramural
Research Support, Non-U.S. Gov't]. 2007;8:60.
43. Geisinger E, Isberg RR. Antibiotic modulation of capsular exopolysaccharide and virulence in Acinetobacter baumannii. PLoS Pathog. [Research Support, N.I.H., Extramural
Research Support, Non-U.S. Gov't]. 2015 Feb;11(2):e1004691.

44. Kulasekara HD, Ventre I, Kulasekara BR, Lazdunski A, Filloux A, Lory S. A novel two-component system controls the expression of Pseudomonas aeruginosa fimbrial cup genes. Mol Microbiol. [Research Support, Non-U.S. Gov't Research Support, U.S. Gov't, P.H.S.]. 2005 Jan;55(2):368-80.

45. Rietsch A, Vallet-Gely I, Dove SL, Mekalanos JJ. ExsE, a secreted regulator of type III secretion genes in Pseudomonas aeruginosa. Proc Natl Acad Sci U S A. [Comparative Study Research Support, N.I.H., Extramural Research Support, Non-U.S. Gov't Research Support, U.S. Gov't, P.H.S.]. 2005 May 31;102(22):8006-11.

46. Chun KT, Edenberg HJ, Kelley MR, Goebl MG. Rapid amplification of uncharacterized transposon-tagged DNA sequences from genomic DNA. Yeast. [Research Support, Non-U.S. Gov't Research Support, U.S. Gov't, P.H.S.]. 1997 Mar 15;13(3):233-40.

47. Suloway C, Pulokas J, Fellmann D, Cheng A, Guerra F, Quispe J, et al. Automated molecular microscopy: the new Leginon system. J Struct Biol. [Research Support, N.I.H., Extramural Research Support, U.S. Gov't, Non-P.H.S. Research Support, U.S. Gov't, P.H.S.]. 2005 Jul;151(1):41-60.

48. Zheng SQ, Palovcak E, Armache JP, Verba KA, Cheng Y, Agard DA. MotionCor2: anisotropic correction of beam-induced motion for improved cryo-electron microscopy. Nat Methods. 2017 Apr;14(4):331-2.

49. Rohou A, Grigorieff N. CTFFIND4: Fast and accurate defocus estimation from electron micrographs. J Struct Biol. [Research Support, Non-U.S. Gov't]. 2015 Nov;192(2):216-21.

50. Lander GC, Stagg SM, Voss NR, Cheng A, Fellmann D, Pulokas J, et al. Appion: an integrated, database-driven pipeline to facilitate EM image processing. J Struct Biol. [Research Support, N.I.H., Extramural Research Support, Non-U.S. Gov't]. 2009 Apr;166(1):95-102.

51. Scheres SH. RELION: implementation of a Bayesian approach to cryo-EM structure determination. J Struct Biol. [Research Support, N.I.H., Extramural Research Support, Non-U.S. Gov't]. 2012 Dec;180(3):519-30.

52. Kimanius D, Forsberg BO, Scheres SH, Lindahl E. Accelerated cryo-EM structure determination with parallelisation using GPUs in RELION-2. Elife. 2016 Nov 15;5.

53. Tang G, Peng L, Baldwin PR, Mann DS, Jiang W, Rees I, et al. EMAN2: an extensible image processing suite for electron microscopy. J Struct Biol. [Evaluation Studies Research Support, N.I.H., Extramural]. 2007 Jan;157(1):38-46.

54. Kelley LA, Mezulis S, Yates CM, Wass MN, Sternberg MJ. The Phyre2 web portal for protein modeling, prediction and analysis. Nat Protoc. [Research Support, Non-U.S. Gov't]. 2015 Jun;10(6):845-58.

55. Pettersen EF, Goddard TD, Huang CC, Couch GS, Greenblatt DM, Meng EC, et al. UCSF Chimera--a visualization system for exploratory research and analysis. J Comput Chem. [Research Support, U.S. Gov't, P.H.S.]. 2004 Oct;25(13):1605-12.

56. DiMaio F, Leaver-Fay A, Bradley P, Baker D, Andre I. Modeling symmetric macromolecular structures in Rosetta3. PLoS One. [Research Support, N.I.H., Extramural

Research Support, Non-U.S. Gov't]. 2011;6(6):e20450.
57. Osborn MJ, Gander JE, Parisi E. Mechanism of assembly of the outer membrane of Salmonella typhimurium. Site of synthesis of lipopolysaccharide. J Biol Chem. 1972 Jun 25;247(12):3973-86.
58. Dalebroux ZD, Edrozo MB, Pfuetzner RA, Ressl S, Kulasekara BR, Blanc MP, et al. Delivery of cardiolipins to the Salmonella outer membrane is necessary for survival within host tissues and virulence. Cell Host Microbe. [Research Support, N.I.H., Extramural Research Support, Non-U.S. Gov't]. 2015 Apr 8;17(4):441-51.
59. Bligh EG, Dyer WJ. A rapid method of total lipid extraction and purification. Can J Biochem Physiol. 1959 Aug;37(8):911-7.
60. MacCoss MJ, Toth MJ, Matthews DE. Evaluation and optimization of ion-current ratio measurements by selected-ion-monitoring mass spectrometry. Anal Chem. [Research Support, U.S. Gov't, P.H.S.]. 2001 Jul 01;73(13):2976-84.

LEGENDS

Figure 1. Disruption of the Mla system results in an altered outer membrane barrier. (**A**) Genomic organization of the *A. baumannii mlaFEDCB* operon and its predicted products. Triangles indicate the position of four independent transposon insertions, isolated in a screen for genes involved in outer membrane integrity. (**B**) Ethidium bromide uptake assay of outer membrane permeability of Δ*mla* mutants and complemented strains. A.U., arbitrary units. Lines shown depect the average of three technical replicates. (**C**) Ethidium bromide uptake assay of outer membrane permeability following plasmid-based expression of MlaF, compared to its dominant negative version, $MlaF^{K55L}$. Lines shown depict the average of three technical replicates. (**D**) Minimum inhibitory concentration (MIC) of select antibiotics in *A. baumannii*. *Indicates wild type *A. baumannii* containing pMMB plasmid constructs, and cultures grown with the addition of kanamycin (25 μg/mL) to maintain plasmids and 50 μM IPTG for induction.

Figure 1 – figure supplement 1. Disruption of the Mla system leads to an increase in exopolysaccharide production. (A) Quantification of crystal violet staining from mla deletion mutants. Error bars represent ± s.d. for biological replicates (n = 3). (B) Quantification of crystal violet staining following plasmid expression of MlaF compared to its dominant negative version, $MlaF^{K55L}$. Error bars represent ± s.d. for biological replicates (n = 3).

Figure 1 – figure supplement 2. Phase microscopy images of wild type and mla mutant *A.*

***baumannii*.** Images were collected from cultures grown to mid-log (OD600 0.4-0.6) growth phase from wild type (A), mlaA (B), mlaC (C), and mlaF (D) deletion mutants of *A. baumannii*.

Figure 2. Structure of the abMlaBDEF complex. (A) Cryo-EM map of abMlaBDEF (grey), with structural models for MlaD, MlaB and MlaF (in magenta, cyan and green respectively) docked at their putative location, as viewed from the side and bottom. The density for most helices is clearly resolved. (B-D) Cartoon representation of the MlaD hexamer (B), the MlaB-MlaF hetero-tetramer (C), and the MlaE dimer (D) region of the MlaBDEFab atomic model . (E) Comparison of the MlaF domain arrangement in the EM map to that of the Maltose transporter ATPase MalK. The two chains of MlaD (in light and dark green) superimpose well to those of MalK (in cyan and dark blue) in the pre- translocation conformation (left, PDB ID: 4KHZ), while a clear rotation is observed compared to the ATP-bound outward-facing conformation (right, PDB ID: 4KI0).

Figure 2 – figure supplement 1. Mla components copurify following protien expression. SDS-PAGE analysis of proteins copurified with hexahistidine-tagged MlaB (-His6). Band identities were assigned based on MS.

Figure 2 – figure supplement 2. Cryo-EM structure of the abMlaBDEF complex. (A) Representative electron micrograph region of frozen-hydrated MlaBDEF complex. The scale bar is in white at the bottom. (B) Representative reference-free 2D class averages of abMlaBDEF, generated using Relion, illustrating the various views observed. (C) Cryo-EM map of the Gpt complex, shown in two orientations corresponding to the two last classes shown in B. (D) The FSC curve for the MlaBDEF structure is shown in black, with the gold-standard resolution definition of 0.143% indicated with a red dotted line. The nominal resolution for this structure is 8.7 Å. (E) The regions of density attributed to the periplasmic domain of MlaD, the TM domains of MlaD and MlaE, and to MlaB and MlaF are in pink, yellow, cyan and green respectively.

Figure 2 – figure supplement 3. Modeling of the abMlaD hexamer. (A) Multiple alignment of MlaD sequences from various gram-negative human pathogens. The secondary structure for ecMlaD is shown at the top. The position of the abMlaD insert is indicated. (B) Result of the all-

atom refinement step for the MlaD hexameric model. The energy of each model is plotted versus the RMSD relative to the initial model and color-coded for the fit to the EM map density. (C) Cartoon representation of our abMlaD hexameric model (magenta), superimposed to the crystallographic ecMlaD hexamer structure (grey).

Figure 2 – figure supplement 4. Close-up view of the MlaB, MlaD, MlaE and MlaF models in the abMlaBDEF cryo-EM map. (A) Region of the density corresponding to a MlaD monomer, with the corresponding atomic model in magenta. The density of the N-terminal helix is well resolved, as well as that of the *A. baumannii*-specific insert. (B) Region of the density corresponding to a MlaF-MlaB hetero-dimer, with the corresponding atomic models in green and cyan respectively, shown from two different angles. Density for helices are well defined for most of the model. (C) Region of the density corresponding to a MlaE monomer, with the corresponding atomic model in yellow.

Figure 3. Localization of the 6 TM helices from MlaD. (A) lateral section of the abMlaBDEF EM map, with the MlaE model in yellow. Density attributed to the MlaD N-terminal helices are indicated with a red star. (B) 2D classes generated from the set of particles used to generate the MlaBDEFab structure, corresponding to side views. A range of orientations for the periplasmic domain is observed. (C) Structure of MlaBDEFab, generated using a subset of the most homogenious ~ 8,000 particles. Some features of the map shown in Figure 3C are not present, but the overall structure is similar. Six well- defined helices in the central TM region are visible. (D) Sections along the vertical axis, corresponding to the three red lines shown in B, is shown on the left. The six- fold axis of MlaD is visible in the periplasmic region, but this breaks down in the TM region, where the six helices are asymmetric. An angular representation of the six helices is represented on the right.

Figure 3 – figure supplement 1. Comparison of the MlaBDEFab and MalBDEFec complex. The map of $MlaBDEF_{ab}$ (this study) is shown in grey, overlaid to that of $MlaBDEF_{ec}$ (ekiert et al.) in yellow, aligned in the cytosolic domains density. The overall architecture of both complexes are similar, however MlaD appears offset by ~ 20 ^{O} in the *A. baumannii* complex, compared to the *E.coli* complex. It remains to be determined if this corresponds to a difference

between species, or if the two structures were obtained in different states of substrate binding and/or nucleotide hydrolysis.

Figure 4. Outer membrane glycerophospholipid levels are reduced in Δ*mlaC* mutant. (**A**) Identification of inner and outer membrane phospholipids of wild type *A. baumannii* and Δ*mlaC* using 2D thin-layer chromatography. PE, phosphatidylethanolamine; PG, phosphatidylglycerol; CL, cardiolipin. (**B**) LC-MS/MS quantification of isolated inner and outer membrane glycerophospholipids. Error bars indicate ± s.e.m. (n = 3).

Figure 4 – figure supplement 1. Purified periplasmic components of the Mla system remain bound to glycerophospholipids. (A) Chromatogram of LC-MS/MS of glycerophospholipids extracted from purified MlaC. Peaks were identified based on MS and elution time. PG, phosphatidylglycerol. PE, phosphatidylethanolamine. (B) Chromatogram of LC-MS/MS of glycerophospholipids extracted from purified MlaD soluble domain.

Figure 4 – figure supplement 2. Deletion of mlaC results in a reduction in levels of outer membrane glycerophospholipids. Total ion scan of isolated outer membranes of A. baumannii and ΔmlaC. Typical membrane glycerophospholipids fall within the m/z range of 600-1500.

Figure 5. Newly synthesized glycerophospholipids accumulate at the inner membrane of Mla mutants. (**A**) LC-MS/MS quantification of ^{13}C labelled/unlabeled glycerophospholipids in isolated membrane fractions over time after growth in 2-^{13}C acetate in Δ*mlaF* and complemented strain. Facet labels on the right indicate the specific glycerophospholipid species analyzed and the acyl chain length. PG, phosphatidylglycerol; PE, phosphatidylethanolamine. Shown is representative data from repeated experiments. (**B**) LC-MS/MS quantification of ^{13}C labelled/un- labeled glycerophospholipids in isolated membrane fractions following plasmid-based expression of MlaF compared to its dominant negative version, MlaF^{K55L}. Facet labels on the right indicate the specific glycerophospholipid species analyzed and the acyl chain length. PG, phosphatidylglycerol; PE, phosphatidylethanolamine. Shown is representative data from repeated experiments. (**C**) Relative proportion of newly synthesized GPL on IM and OM after one hour growth in 2-^{13}C acetate. Error bars represent ± s.d. (n = 2). Statistical analyses

performed using a Student's *t* test. *p*-Value: *, $p < 0.05$; **, $p < 0.01$.

Figure 5 – figure supplement 1. A stable isotope assay of glycerophospholipid transport from the inner membrane to the outer membrane. (A) Schematic showing an example of the shift in mass-to-charge ratio (m/z) of glycerophospholipids (GPL) following growth in 2-^{13}C acetate. (B) A schematic illustrating the rationale of the stable isotope assay: (1) Newly synthesized ^{13}C-labeled GPL, shown here in red, are first inserted into the inner membrane (IM) following synthesis; (2) the likelihood that a given GPL that is trafficked from the IM to the OM will be labeled is proportional to the ratio of labeled to unlabeled GPL in the IM; (3) a comparison of the ratios of labeled to unlabeled GPL in the inner and outer membranes will therefore reflect the efficiency of GPL transport.

Figure 5 – figure supplement 2. Newly synthesized glycerophospholipids accumulate at the inner membrane of MlaA mutants. (A) LC-MS/MS quantification of ^{13}C labelled/unlabeled glycerophospholipids in isolated membrane fractions over time after growth in 2-^{13}C acetate in ΔmlaC and complemented strain. Facet labels on the right indicate the specific glycerophospholipid species analyzed and the acyl chain length. PG, phosphatidylglycerol; PE, phosphatidylethanolamine. Shown is representative data from repeated experiments. (B) LC-MS/MS quantification of ^{13}C labelled/unlabeled glycerophospholipids in isolated membrane fractions over time after growth in 2-^{13}C acetate in ΔmlaF and complemented strain. Facet labels on the right indicate the specific glycerophospholipid species analyzed and the acyl chain length. PG, phosphatidylglycerol; PE, phosphatidylethanolamine. Shown is representative data from repeated experiments. (C) Relative proportion of newly synthesized GPL on IM and OM after one hour growth in 2-^{13}C acetate. Error bars represent ± s.d. (n = 2). Statistical analyses performed using a Student's t test. p-Value: *, $p < 0.05$; **, $p < 0.01$.

Figure 5 – figure supplement 3. Confirmation of inner and outer membrane separation. Each lane contains 10 µg total protein as measured by Bradford protein assay. (A) α-OmpA Western blot of separated membranes analyzed in Figure 4. (B) α-OmpA Western blot of separated membranes analyzed in Figure 5A (C) α-OmpA Western blot of separated membranes analyzed in Figure 5B. (D) α-OmpA Western blot of separated membranes analyzed in Figure

5C. (E) Coomasie stained SDS-protein gel of representative isolated membrane samples alongside BioRad Precision Plus Protein Standard. (F) Separation of inner and outer membranes into distinct bands by 3-step sucrose gradient. (G) NADH assay for enzymatic activity of inner membrane.

Figure 6. The multicomponent Mla system transports glycerophospholipids from the inner membrane to the outer membrane of *A. baumannii.* A schematic of glycerophospholipid transport to the Gram-negative bacterial outer membrane by the Mla system.

Supplemental File 1: Results of transposon mutagenesis screen for genes involved in outer membrane barrier function in ATCC 17978

Supplemental File 2: Accumulation of newly synthesized glycerophospholipids in *A. baumannii* inner and outer membranes

A

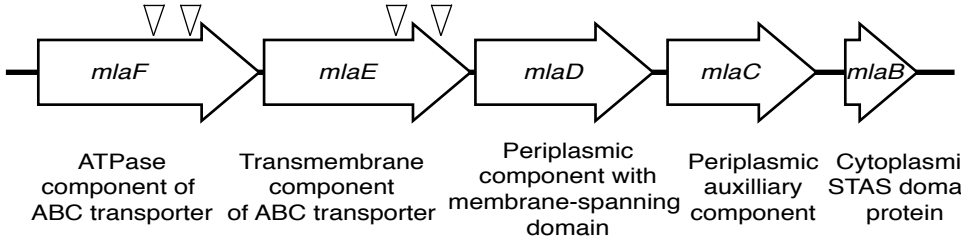

B

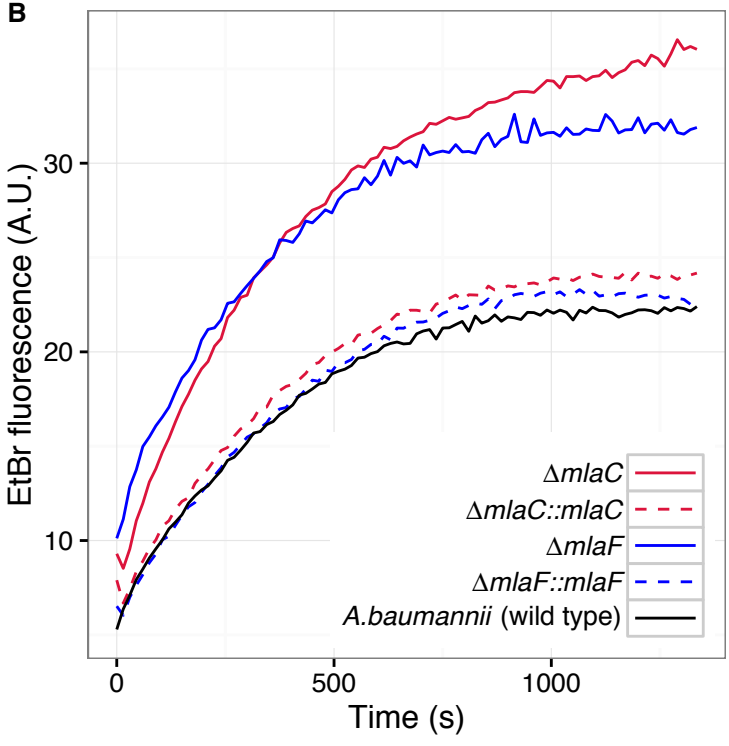

C

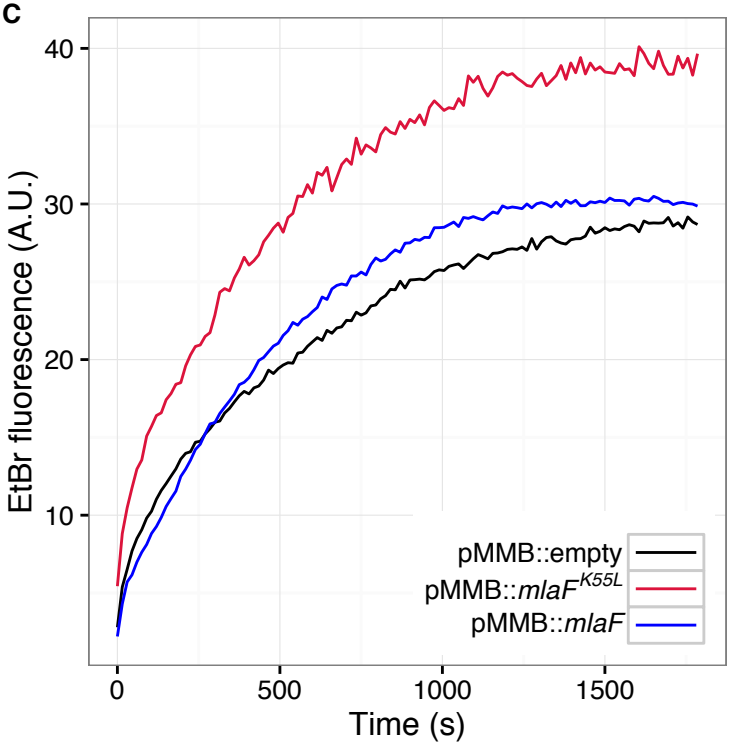

D

	MIC (μg/mL)		
	Gentamicin	Novobicin	Rifampicin
A. baumannii	16.00	3.91	1.60
Δ*mlaC*	7.80	0.49	0.05
Δ*mlaC::mlaC*	16.0	3.91	1.60
Δ*mlaF*	7.80	0.49	0.05
Δ*mlaF::mlaF*	16.0	3.91	1.60
pMMB::empty*	7.80	0.78	0.78
pMMB::mla*F**	7.80	0.78	0.78
pMMB::mla*F-K55L**	3.91	0.20	0.20

Fig. 1. Disruption of the Mla system results in an altered outer membrane barrier. (**A**) Genomic organization of the *A. baumannii mlaFEDCB* operon and its predicted products. Triangles indicate the position of four independent transposon insertions, isolated in a screen for genes involved in outer membrane integrity. (**B**) Ethidium bromide uptake assay of outer membrane permeability of Δ*mla* mutants and complemented strains. A.U., arbitrary units. Lines shown depect the average of three technical replicates. (**C**) Ethidium bromide uptake assay of outer membrane permeability following plasmid-based expression of MlaF, compared to its dominant negative version, MlaF^{K55L}. Lines shown depict the average of three technical replicates. (**D**) Minimum inhibitory concentration (MIC) of select antibiotics in *A. baumannii*. *Indicates wild type *A. baumannii* containing pMMB plasmid constructs, and cultures grown with the addition of kanamycin (25 μg/mL) to maintain plasmids and 50 μM IPTG for induction.

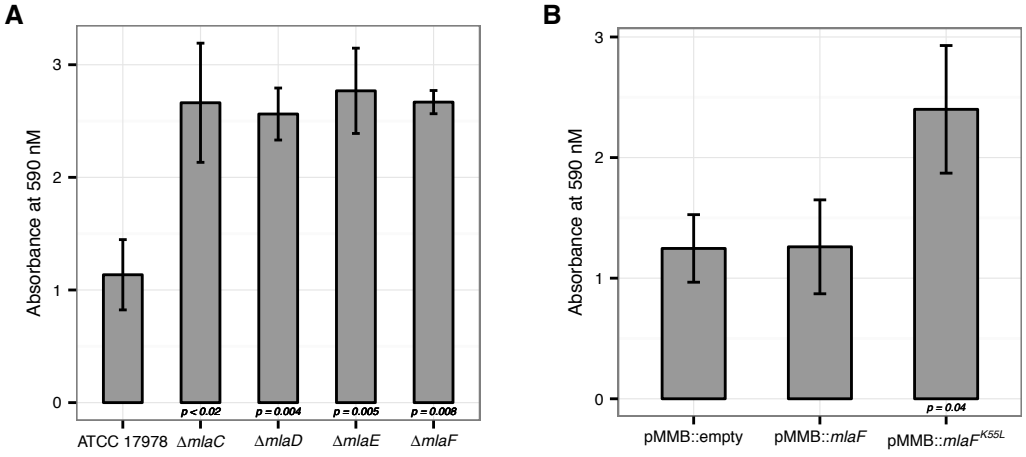

Figure 1 - figure supplement 1. Disruption of the Mla system leads to an increase in exopolysaccharide production. (**A**) Quantification of crystal violet staining from *mla* deletion mutants. Error bars represent ± s.d. for biological replicates (n = 3). (**B**) Quantification of crystal violet staining following plasmid expression of MlaF compared to its dominant negative version, MlaF^{K55L}. Error bars represent ± s.d. for biological replicates (n = 3).

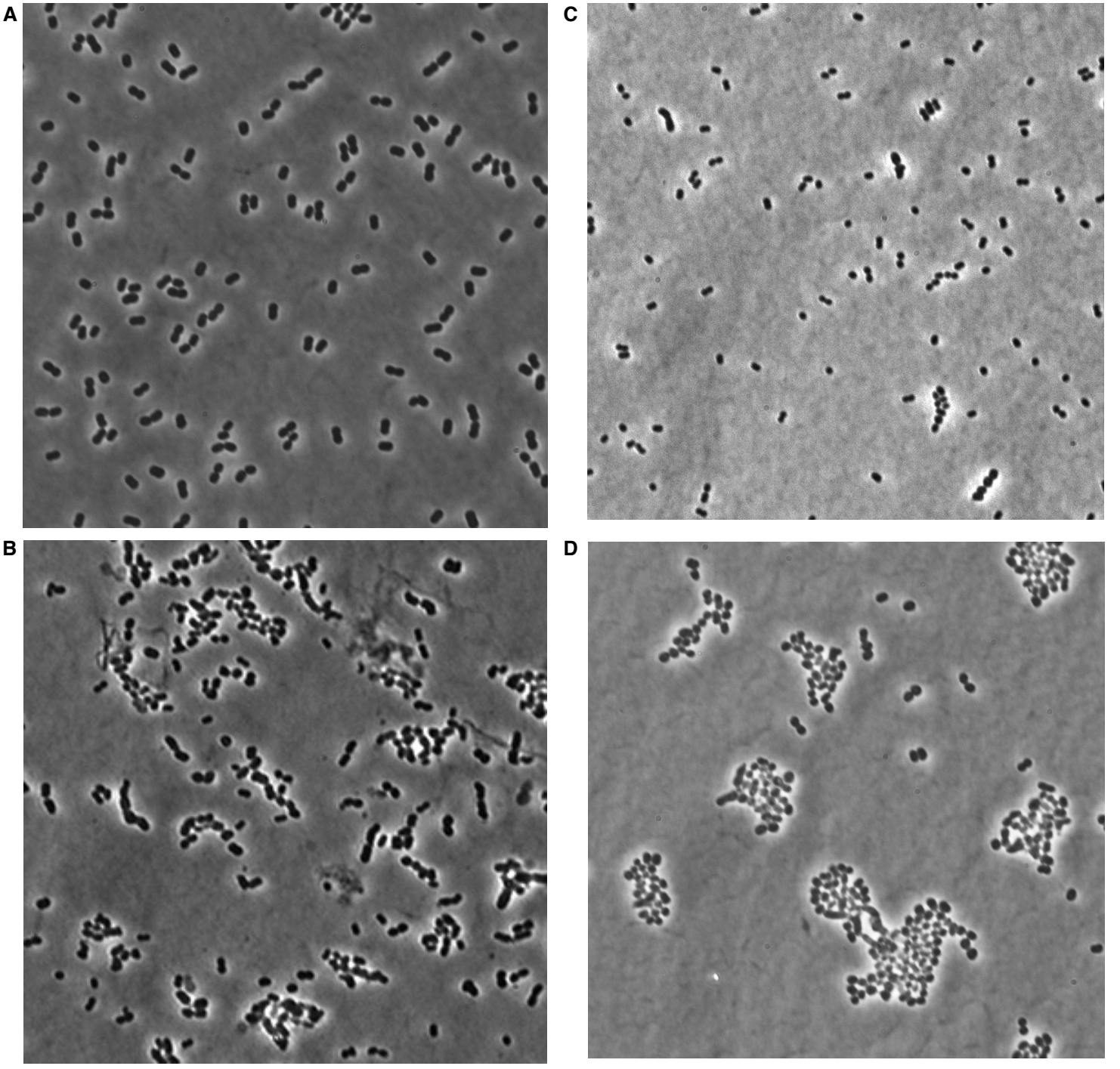

Figure 1 - figure supplement 2. Phase microscopy images of wild type and *mla* mutant *A. baumannii*. Images were collected from cultures grown to mid-log (OD600 0.4-0.6) growth phase from wild type (**A**), *mlaA* (**B**), *mlaC* (**C**), and *mlaF* (**D**) deletion mutants of *A. baumannii*.

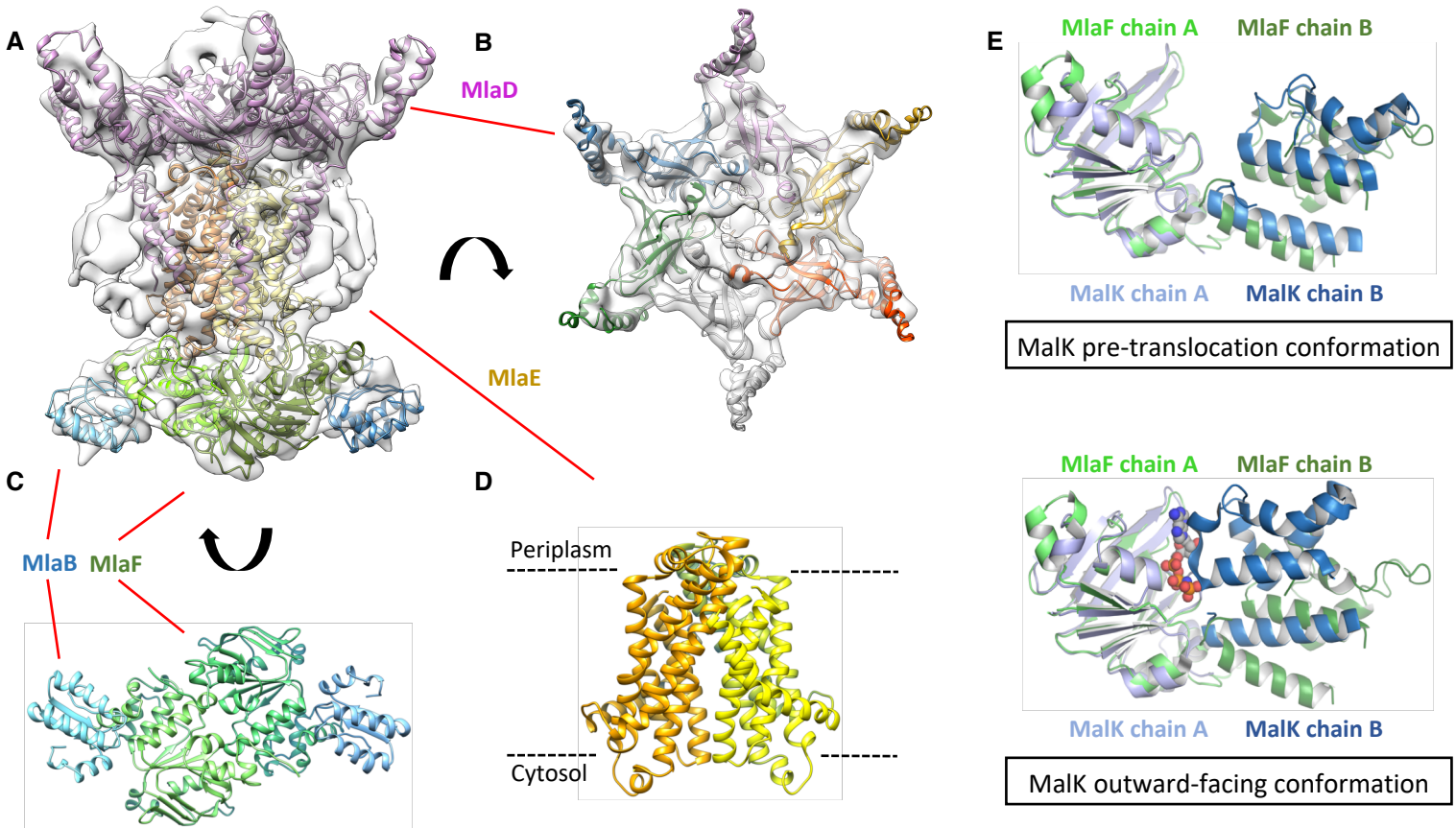

Fig. 2. Structure of the abMlaBDEF complex. (**A**) Cryo-EM map of abMlaBDEF (grey), with structural models for MlaD, MlaB and MlaF (in magenta, cyan and green respectively) docked at their putative location, as viewed from the side and bottom. The density for most helices is clearly resolved. (**B-D**) Cartoon representation of the MlaD hexamer (**B**), the MlaB-MlaF hetero-tetramer (**C**), and the MlaE dimer (**D**) region of the $MlaBDEF_{ab}$ atomic model . (**E**) Comparison of the MlaF domain arrangement in the EM map to that of the Maltose transporter ATPase MalK. The two chains of MlaD (in light and dark green) superimpose well to those of MalK (in cyan and dark blue) in the pre- translocation conformation (left, PDB ID: 4KHZ), while a clear rotation is observed compared to the ATP-bound outward-facing conformation (right, PDB ID: 4KI0).

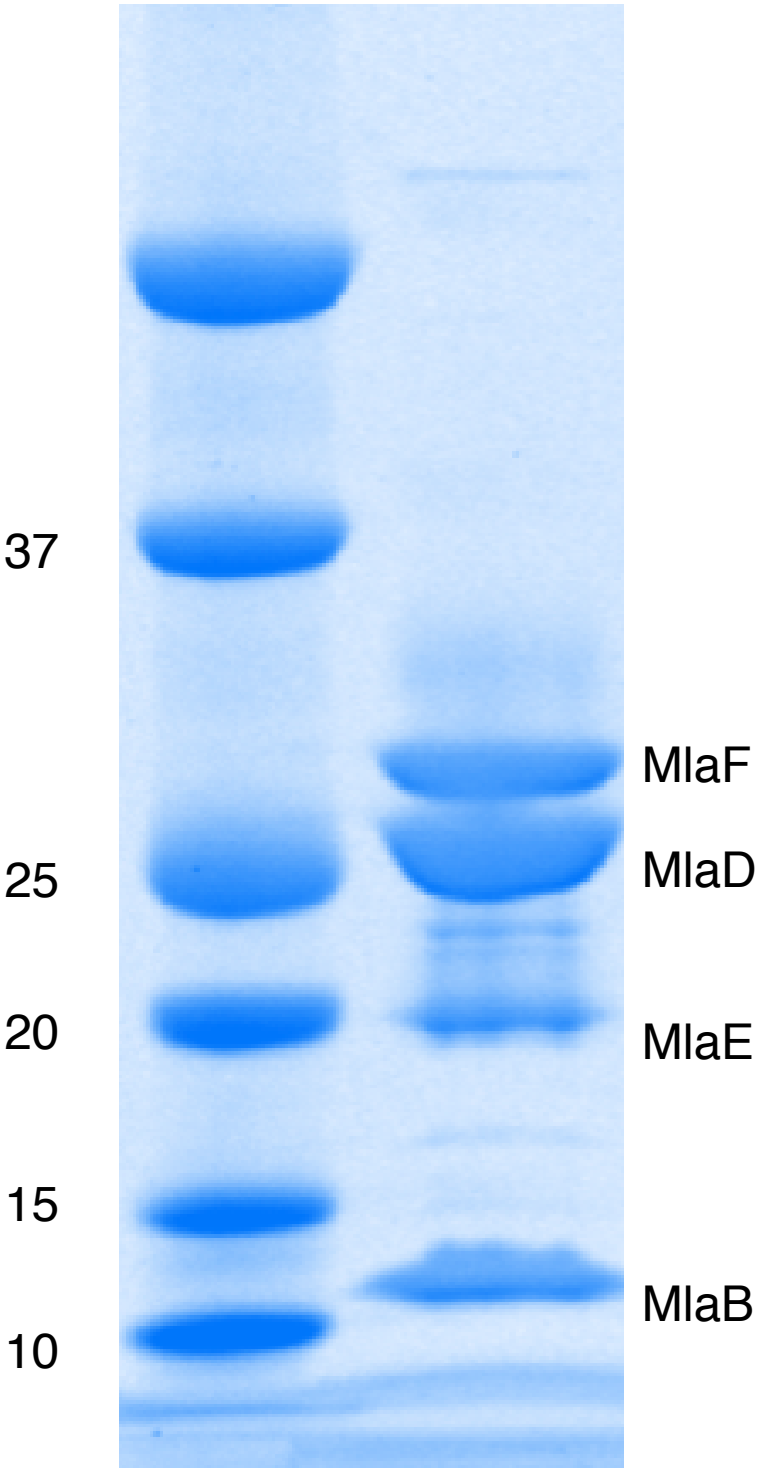

Figure 2 - figure supplement 1. Mla components copurify following protien expression. SDS-PAGE analysis of proteins copurified with hexahistidine-tagged MlaB (-His6). Band identities were assigned based on MS.

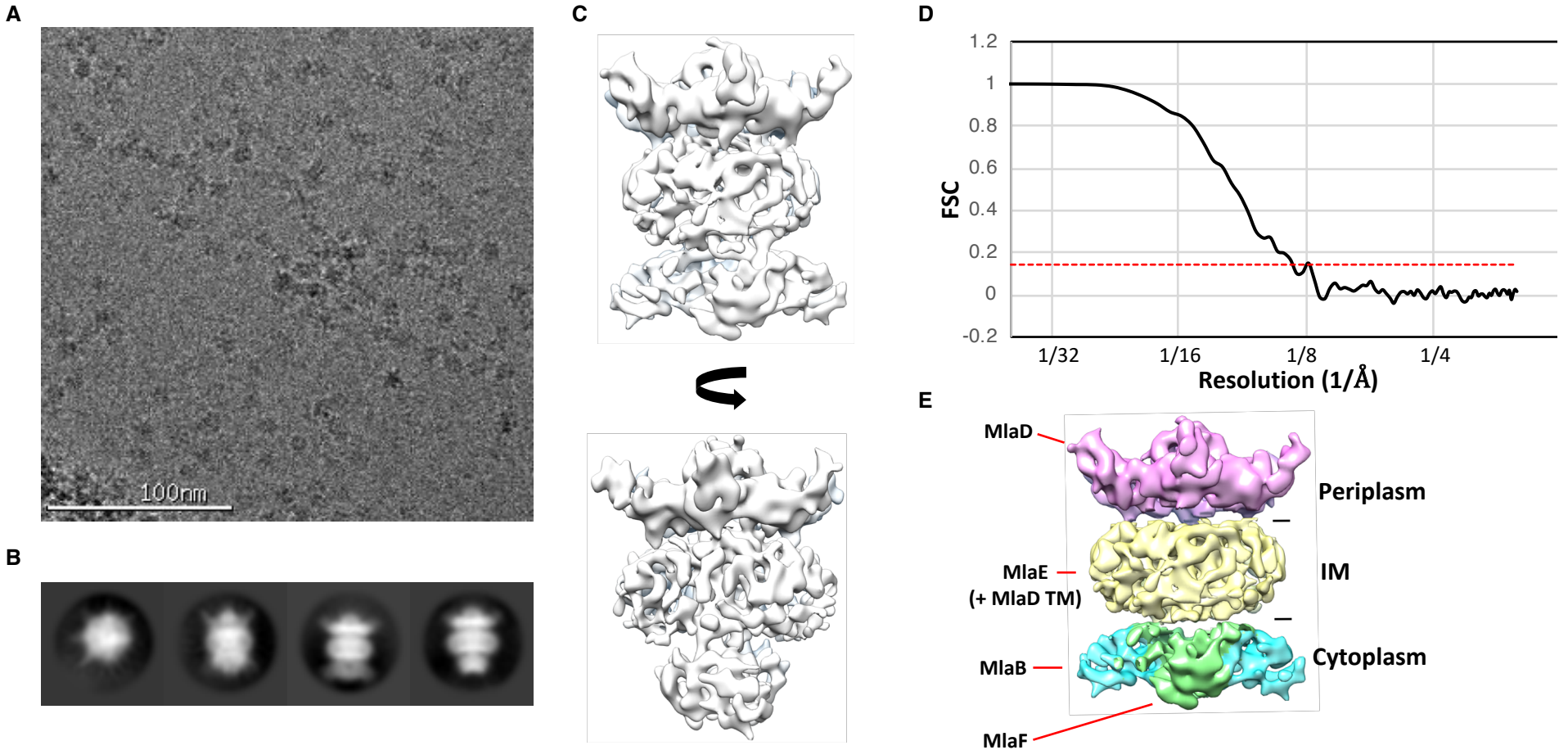

Figure 2 - figure supplement 2. Cryo-EM structure of the abMlaBDEF complex. (**A**) Representative electron micrograph region of frozen-hydrated MlaBDEF complex. The scale bar is in white at the bottom. (**B**) Representative reference-free 2D class averages of abMlaBDEF, generated using Relion, illustrating the various views observed. (**C**) Cryo-EM map of the Gpt complex, shown in two orientations corresponding to the two last classes shown in B. (**D**) The FSC curve for the MlaBDEF structure is shown in black, with the gold-standard resolution definition of 0.143% indicated with a red dotted line. The nominal resolution for this structure is 8.7 Å. (**E**) The regions of density attributed to the periplasmic domain of MlaD, the TM domains of MlaD and MlaE, and to MlaB and MlaF are in pink, yellow, cyan and green respectively.

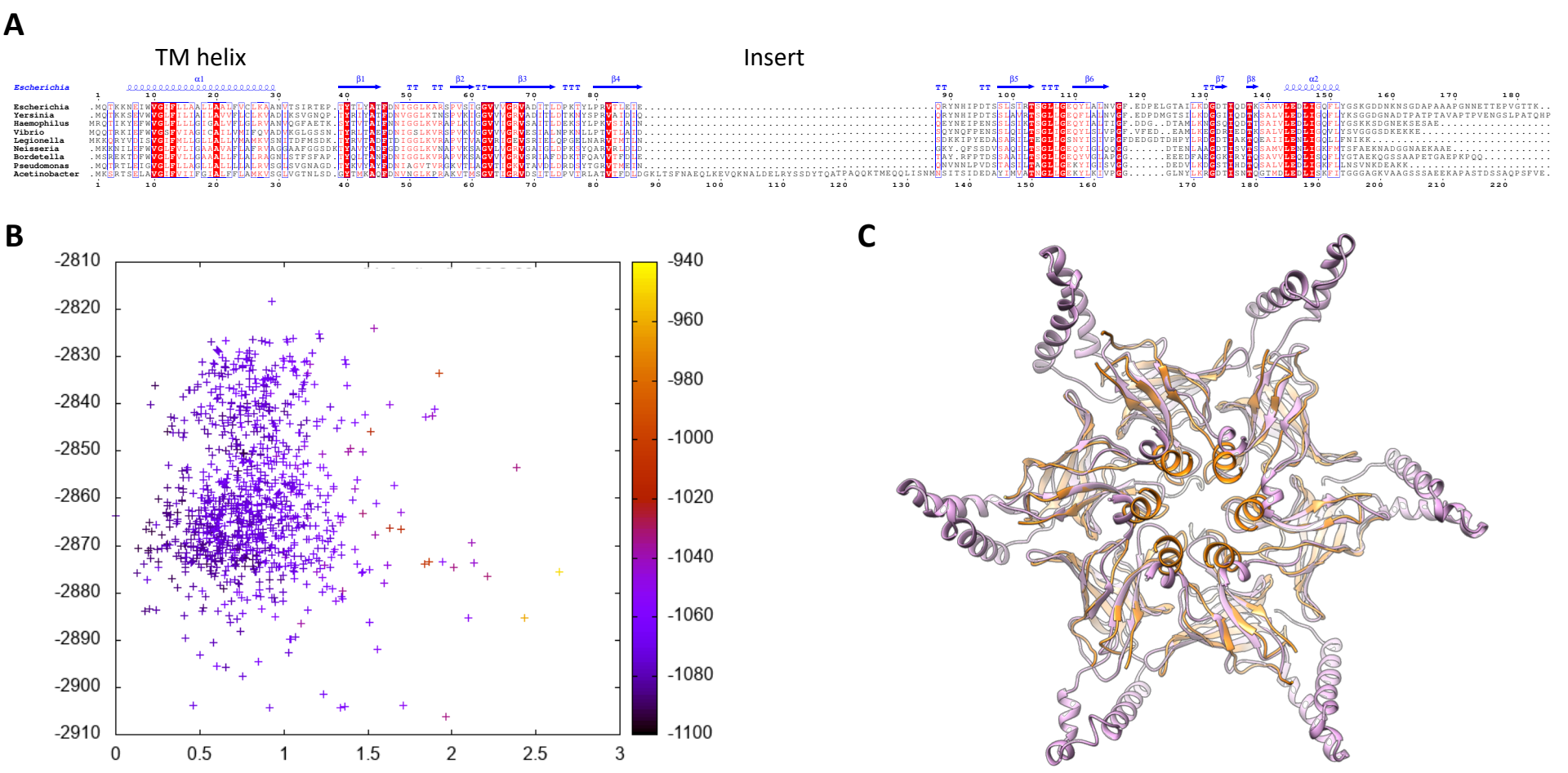

Figure 2 - figure supplement 3. Modeling of the abMlaD hexamer. (**A**) Multiple alignment of MlaD sequences from various gram-negative human pathogens. The secondary structure for ecMlaD is shown at the top. The position of the abMlaD insert is indicated. (**B**) Result of the all-atom refinement step for the MlaD hexameric model. The energy of each model is plotted versus the RMSD relative to the initial model, and color-coded for the fit to the EM map density. (**C**) Cartoon representation of our abMlaD hexameric model (magenta), superimposed to the crystallographic ecMlaD hexamer structure (grey).

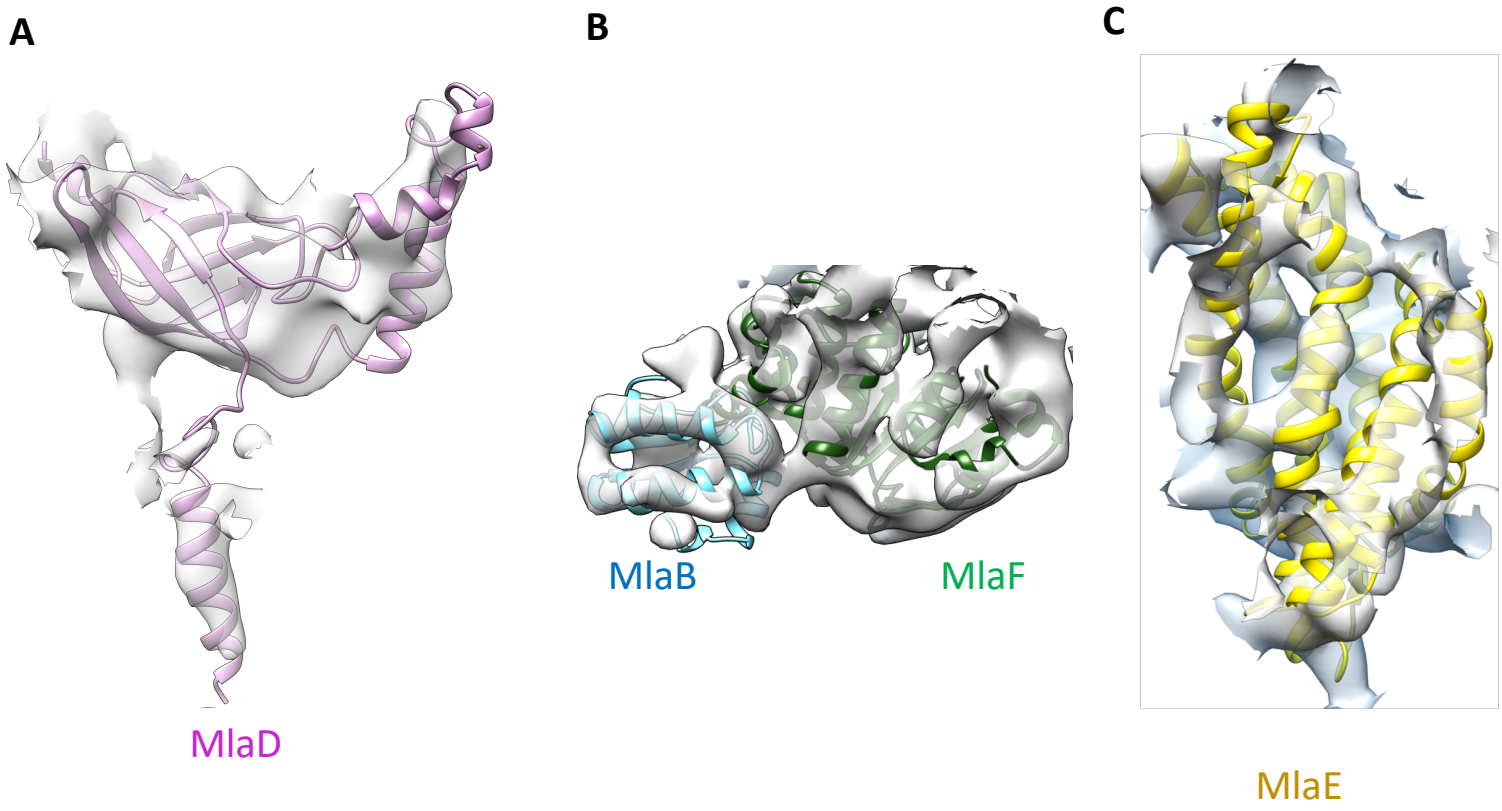

Figure 2 - figure supplement 4. Close-up view of the MlaB, MlaD, MlaE and MlaF models in the abMlaBDEF cryo-EM map. (**A**) Region of the density corresponding to a MlaD monomer, with the corresponding atomic model in magenta. The density of the N-terminal helix is well resolved, as well as that of the A. baumannii-specific insert. (**B**) Region of the density corresponding to a MlaF-MlaB hetero-dimer, with the corresponding atomic models in green and cyan respectively, shown from two different angles. Density for helices are well defined for most of the model. (**C**) Region of the density corresponding to a MlaE monomer, with the corresponding atomic model in yellow.

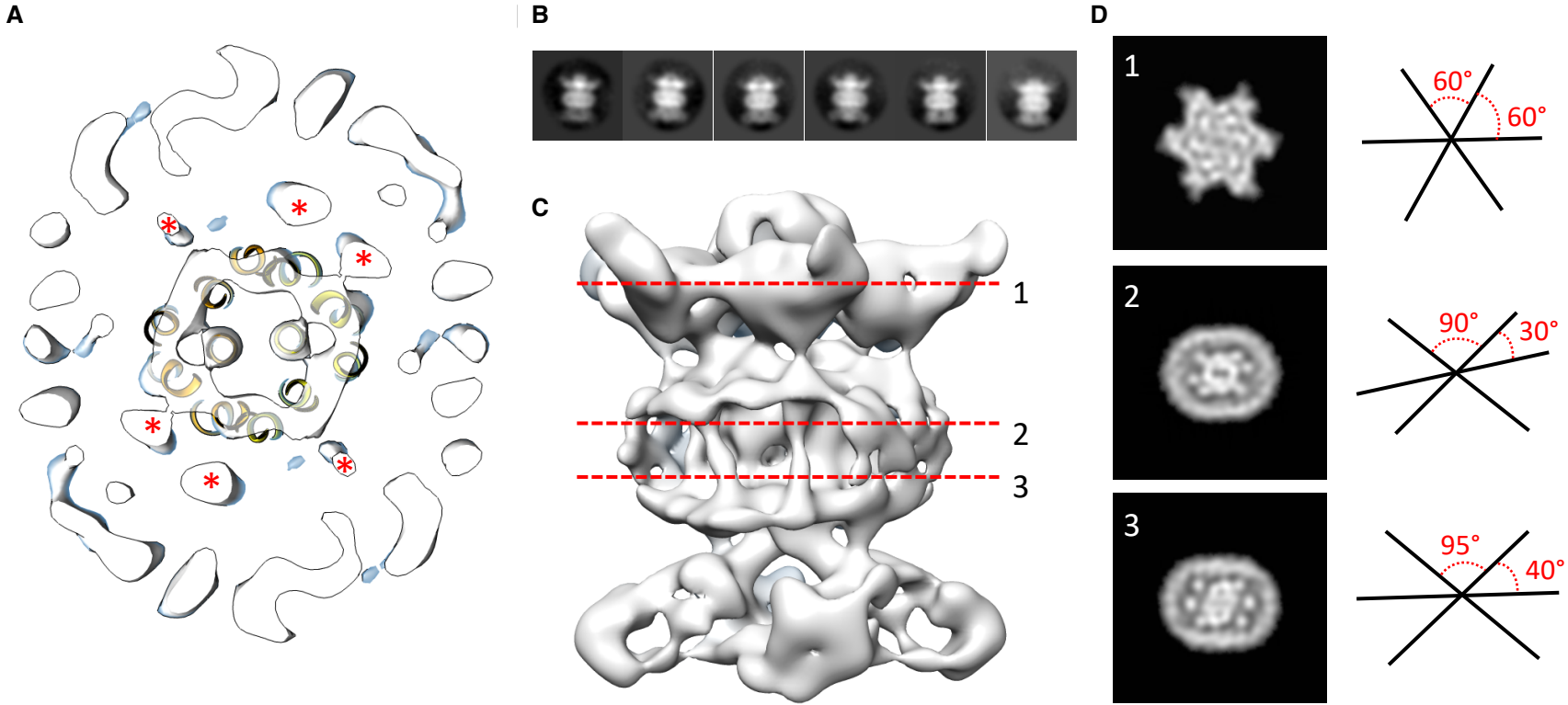

Fig. 3. Localization of the 6 TM helices from MlaD. (**A**) lateral section of the abMlaBDEF EM map, with the MlaE model in yellow. Density attributed to the MlaD N-terminal helices are indicated with a red star. (**B**) 2D classes generated from the set of particles used to generate the $MlaBDEF_{ab}$ structure, corresponding to side views. A range of orientations for the periplasmic domain is observed. (**C**) Structure of $MlaBDEF_{ab}$, generated using a subset of the most homogenious ~ 8,000 particles. Some features of the map shown in Figure 3C are not present, but the overall structure is similar. Six well- defined helices in the central TM region are visible. (**D**) Sections along the vertical axis, corresponding to the three red lines shown in B, is shown on the left. The six- fold axis of MlaD is visible in the periplasmic region, but this breaks down in the TM region, where the six helices are asymmetric. An angular representation of the six helices is represented on the right.

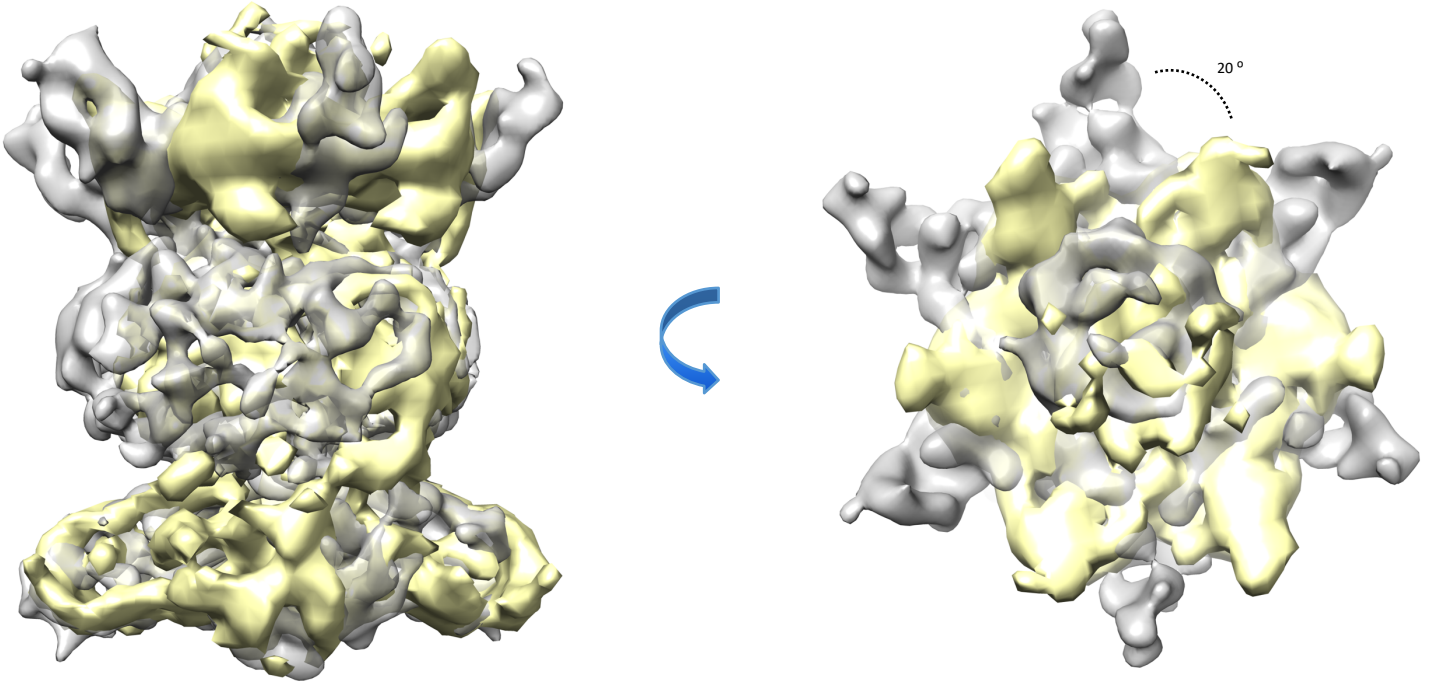

Figure 3 - figure supplement 1. Comparison of the MlaBDEF$_{ab}$ and MalBDEF$_{ec}$ complex. The map of MlaBDEFab (this study) is shown in grey, overlaid to that of MlaBDEF$_{ec}$ (ekiert et al.) in yellow, aligned in the cytosolic domains density. The overall architecture of both complexes are similar, however MlaD appears offset by ~ 20 ^{O} in the *A. baumannii* complex, compared to the *E.coli* complex. It remains to be determined if this corresponds to a difference between species, or if the two structures were obtained in different states of substrate binding and/or nucleotide hydrolysis.

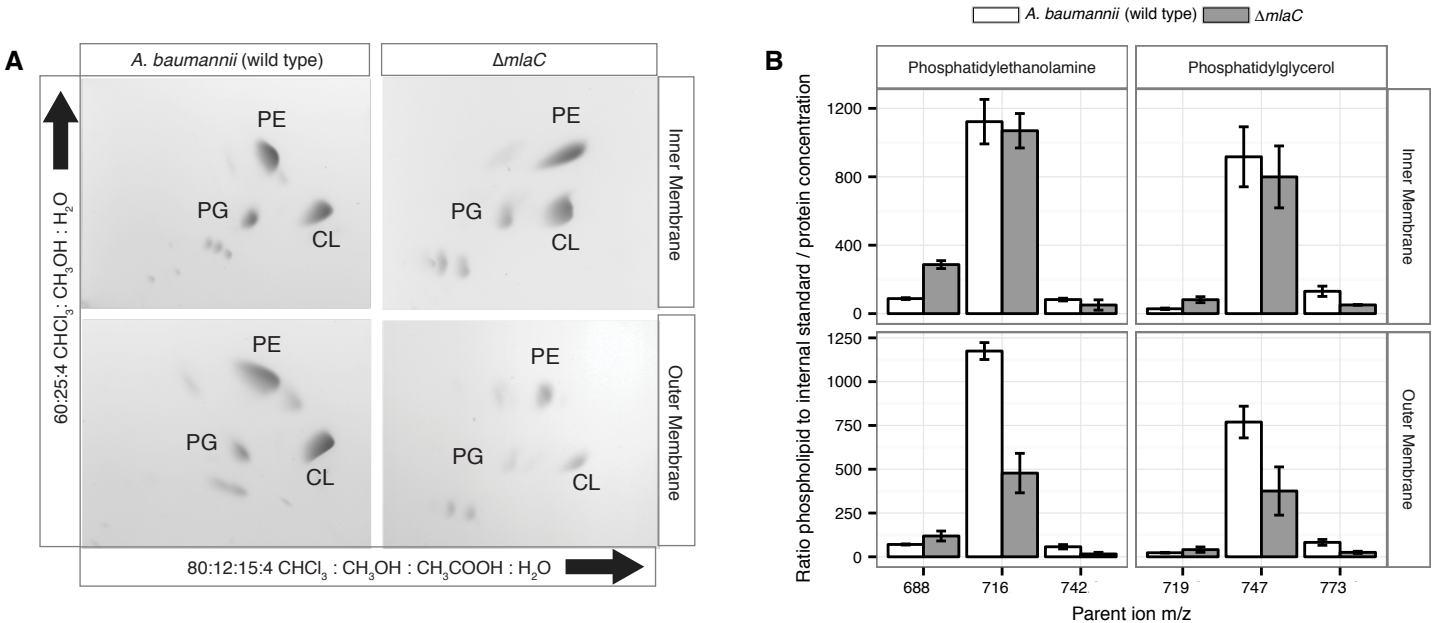

Fig 4. Outer membrane glycerophospholipid levels are reduced in Δ*mlaC* mutant. (**A**) Identification of inner and outer membrane phospholipids of wild type *A. baumannii* and Δ*mlaC* using 2D thin-layer chromatography. PE, phosphatidylethanolamine; PG, phosphatidylglycerol; CL, cardiolipin. (**B**) LC-MS/MS quantification of isolated inner and outer membrane glycerophospholipids. Error bars indicate ± s.e.m. (n = 3).

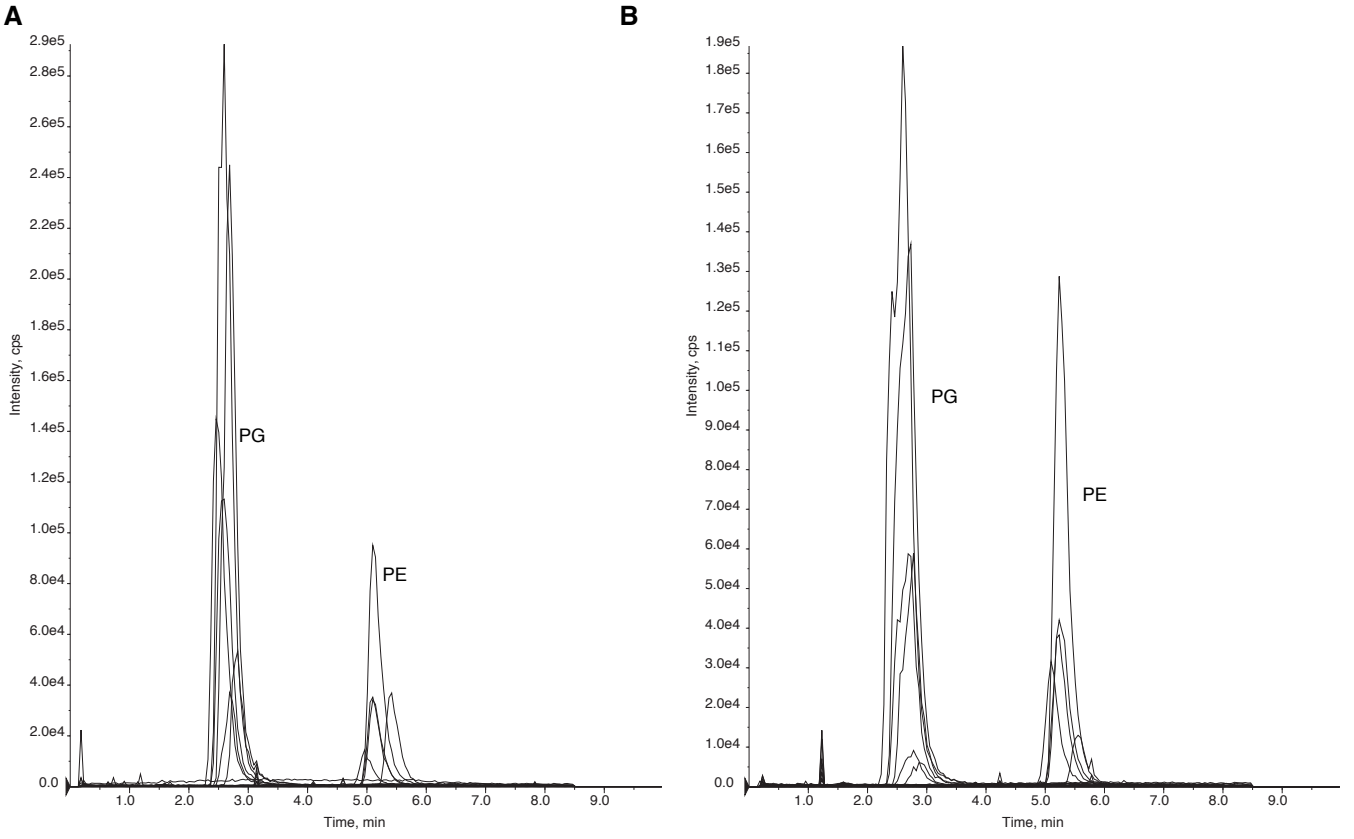

Figure 4 - figure supplement 1. Purified periplasmic components of the Mla system remain bound to glycerophospholipids. (**A**) Chromatogram of LC-MS/MS of glycerophospholipids extracted from purified MlaC. Peaks were identified based on MS and elution time. PG, phosphatidylglycerol. PE, phosphatidylethanolamine. (**B**) Chromatogram of LC-MS/MS of glycerophospholipids extracted from purified MlaD soluble domain.

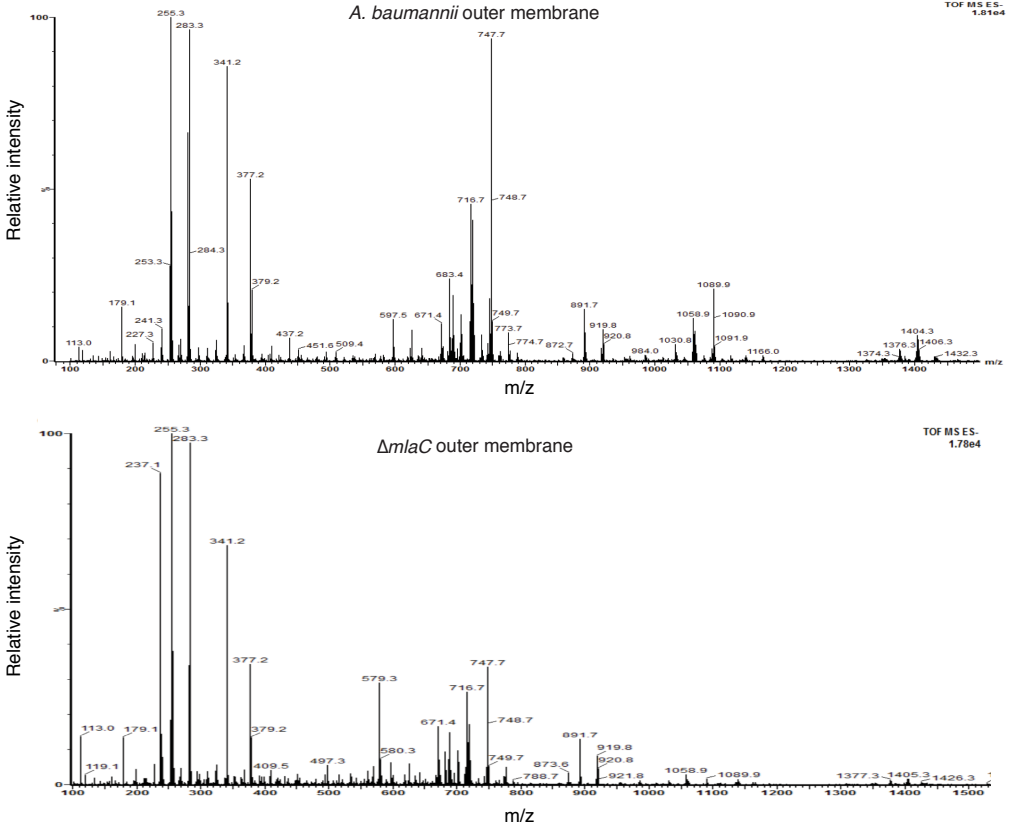

Figure 4 - figure supplement 2. Deletion of *mlaC* results in a reduction in levels of outer membrane glycerophospholipids. Total ion scan of isolated outer membranes of *A. baumannii* and Δ*mlaC*. Typical membrane glycerophospholipids fall within the m/z range of 600-1500.

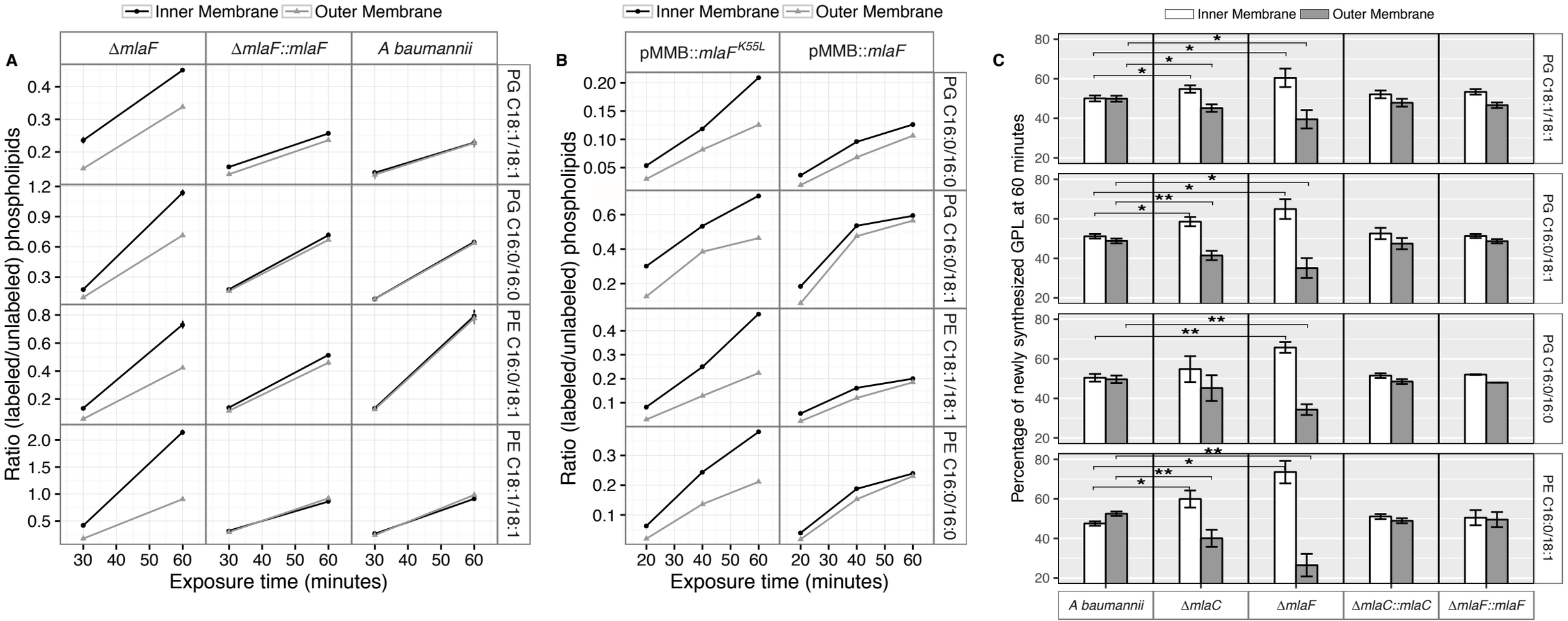

Fig. 5. Newly synthesized glycerophospholipids accumulate at the inner membrane of Mla mutants. (**A**) LC-MS/MS quantification of ^{13}C labelled/unlabeled glycerophospholipids in isolated membrane fractions over time after growth in 2-^{13}C acetate in Δ*mlaF* and complemented strain. Facet labels on the right indicate the specific glycerophospholipid species analyzed and the acyl chain length. PG, phosphatidylglycerol; PE, phosphatidylethanolamine. Shown is representative data from repeated experiments. Error bars represent ± s.d. (n = 2) for technical replicates. (**B**) LC-MS/MS quantification of ^{13}C labelled/unlabeled glycerophospholipids in isolated membrane fractions following plasmid-based expression of MlaF compared to its dominant negative version, MlaF^{K55L}. Facet labels on the right indicate the specific glycerophospholipid species analyzed and the acyl chain length. PG, phosphatidylglycerol; PE, phosphatidylethanolamine. Shown is representative data from repeated experiments. (**C**) Relative proportion of newly synthesized GPL on IM and OM after one hour growth in 2-^{13}C acetate. Error bars represent ± s.d. (n = 2). Statistical analyses performed using a Student's t test. p-Value: *, $p < 0.05$; **, $p < 0.01$.

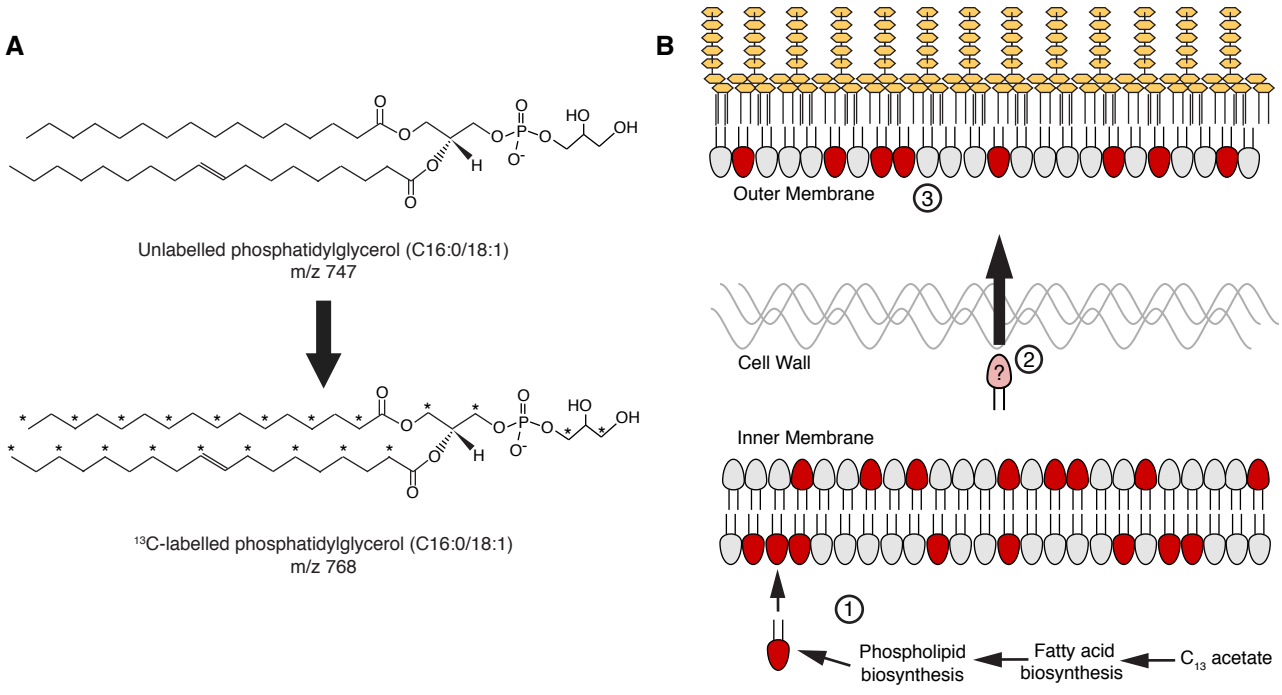

Figure 5 - figure supplement 1. A stable isotope assay of glycerophospholipid transport from the inner membrane to the outer membrane (**A**) Schematic showing an example of the shift in mass-to-charge ratio (m/z) of glycerophospholipids (GPL) following growth in 2-^{13}C acetate. (**B**) A schematic illustrating the rationale of the stable isotope assay: (1) Newly synthesized ^{13}C-labeled GPL, shown here in red, are first inserted into the inner membrane (IM) following synthesis; (2) the likelihood that a given GPL that is trafficked from the IM to the OM will be labeled is proportional to the ratio of labeled to unlabeled GPL in the IM; (3) a comparison of the ratios of labeled to unlabeled GPL in the inner and outer membranes will therefore reflect the efficiency of GPL transport.

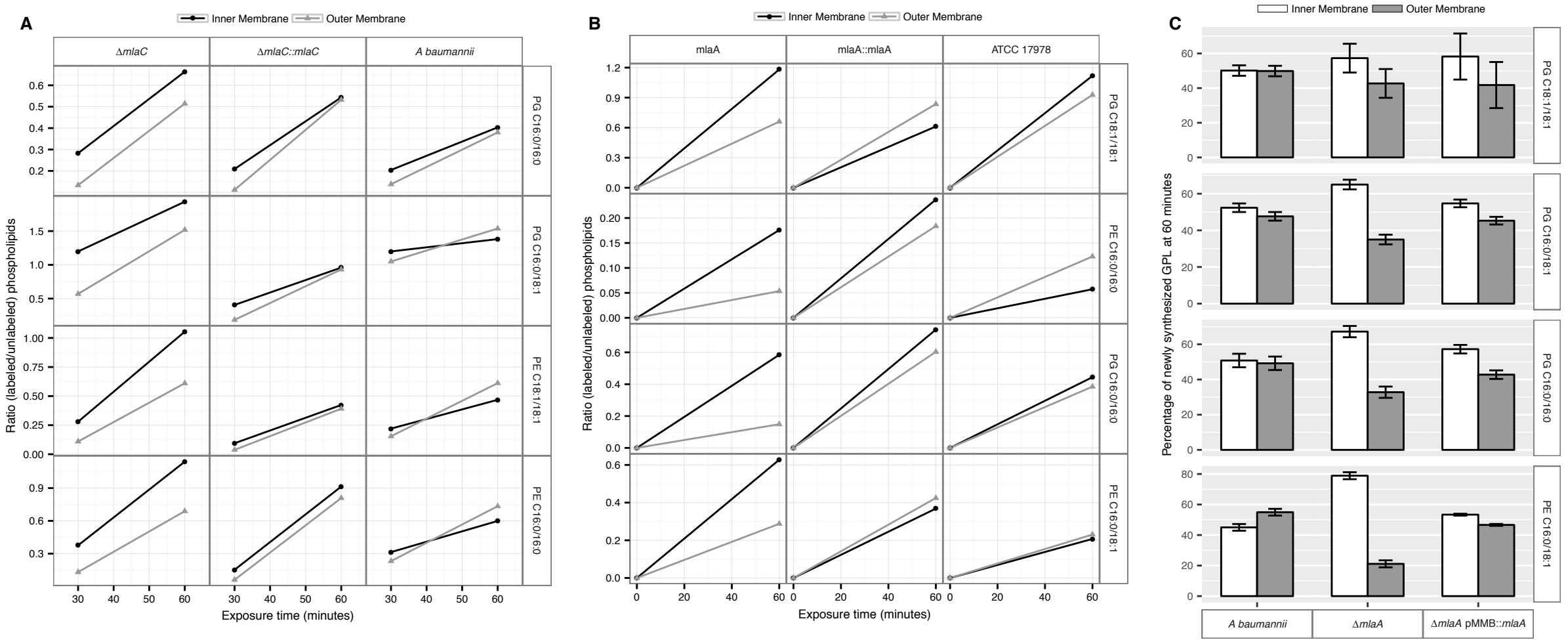

Figure 5 - figure supplement 2. Newly synthesized glycerophospholipids accumulate at the inner membrane of MlaA mutants. (**A**) LC-MS/MS quantification of ^{13}C labelled/unlabeled glycerophospholipids in isolated membrane fractions over time after growth in 2-^{13}C acetate in Δ*mlaC* and complemented strain. Facet labels on the right indicate the specific glycerophospholipid species analyzed and the acyl chain length. PG, phosphatidylglycerol; PE, phosphatidylethanolamine. Shown is representative data from repeated experiments. (B) LC-MS/MS quantification of ^{13}C labelled/unlabeled glycerophospholipids in isolated membrane fractions over time after growth in 2-^{13}C acetate in ΔmlaF and complemented strain. Facet labels on the right indicate the specific glycerophospholipid species analyzed and the acyl chain length. PG, phosphatidylglycerol; PE, phosphatidylethanolamine. Shown is representative data from repeated experiments. (C) Relative proportion of newly synthesized GPL on IM and OM after one hour growth in 2-^{13}C acetate. Error bars represent ± s.d. (n = 2). Statistical analyses performed using a Student's t test. p-Value: *, $p < 0.05$; **, $p < 0.01$.

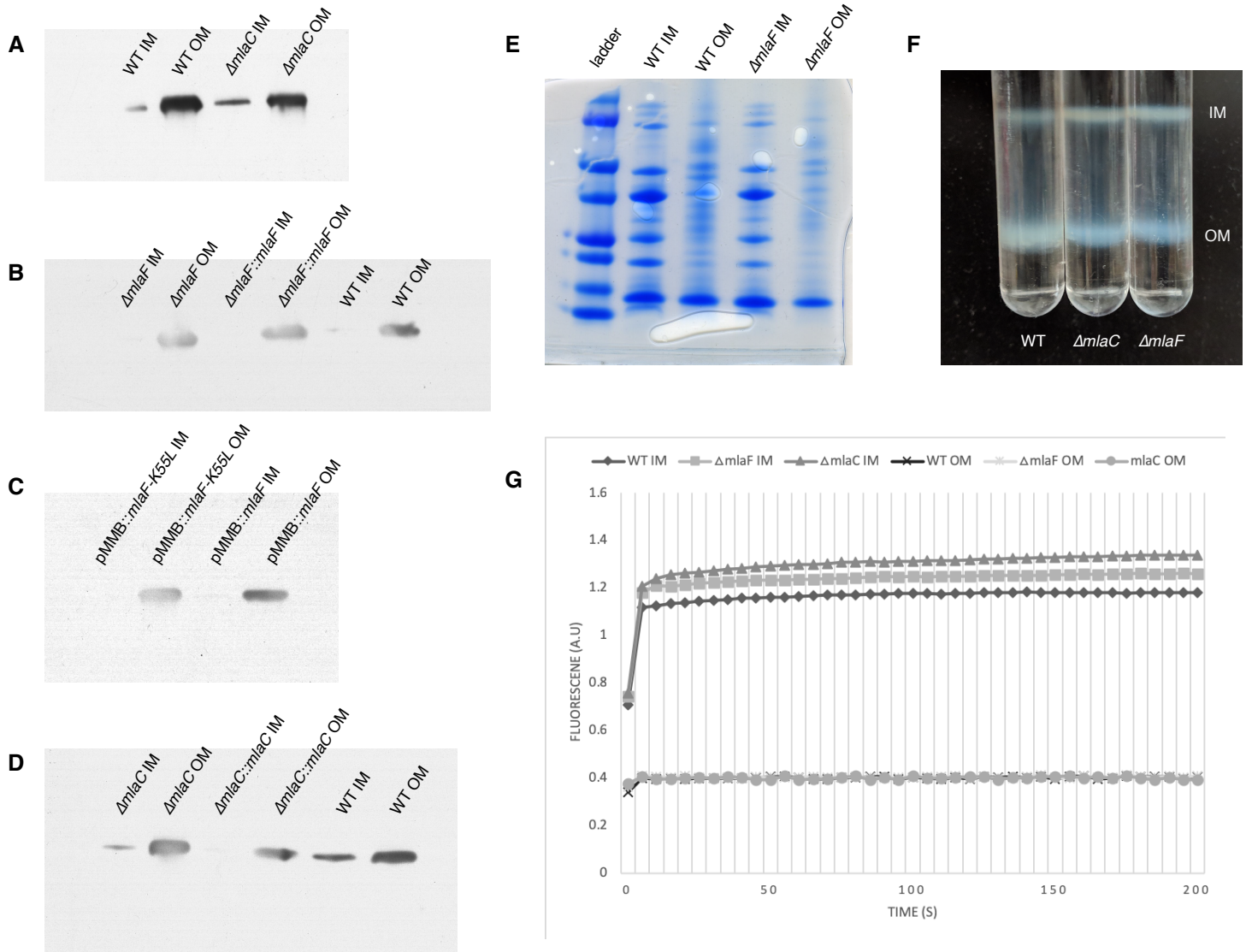

Figrue 5 - figure supplement 3. Confirmation of inner and outer membrane separation. Each lane contains 10 μg total protein as measured by Bradford protein assay. (**A**) α-OmpA Western blot of separated membranes analyzed in Figure 4. (**B**) α-OmpA Western blot of separated membranes analyzed in Figure 5A (**C**) α-OmpA Western blot of separated membranes analyzed in Figure 5B. (**D**) α-OmpA Western blot of separated membranes analyzed in Figure 5C. (**E**) Coomasie stained SDS-protein gel of representative isolated membrane samples alongside BioRad Precision Plus Protein Standard. (**F**) Separation of inner and outer membranes into distinct bands by 3-step sucrose gradient. (**G**) NADH assay for enzymatic activity of inner membrane.

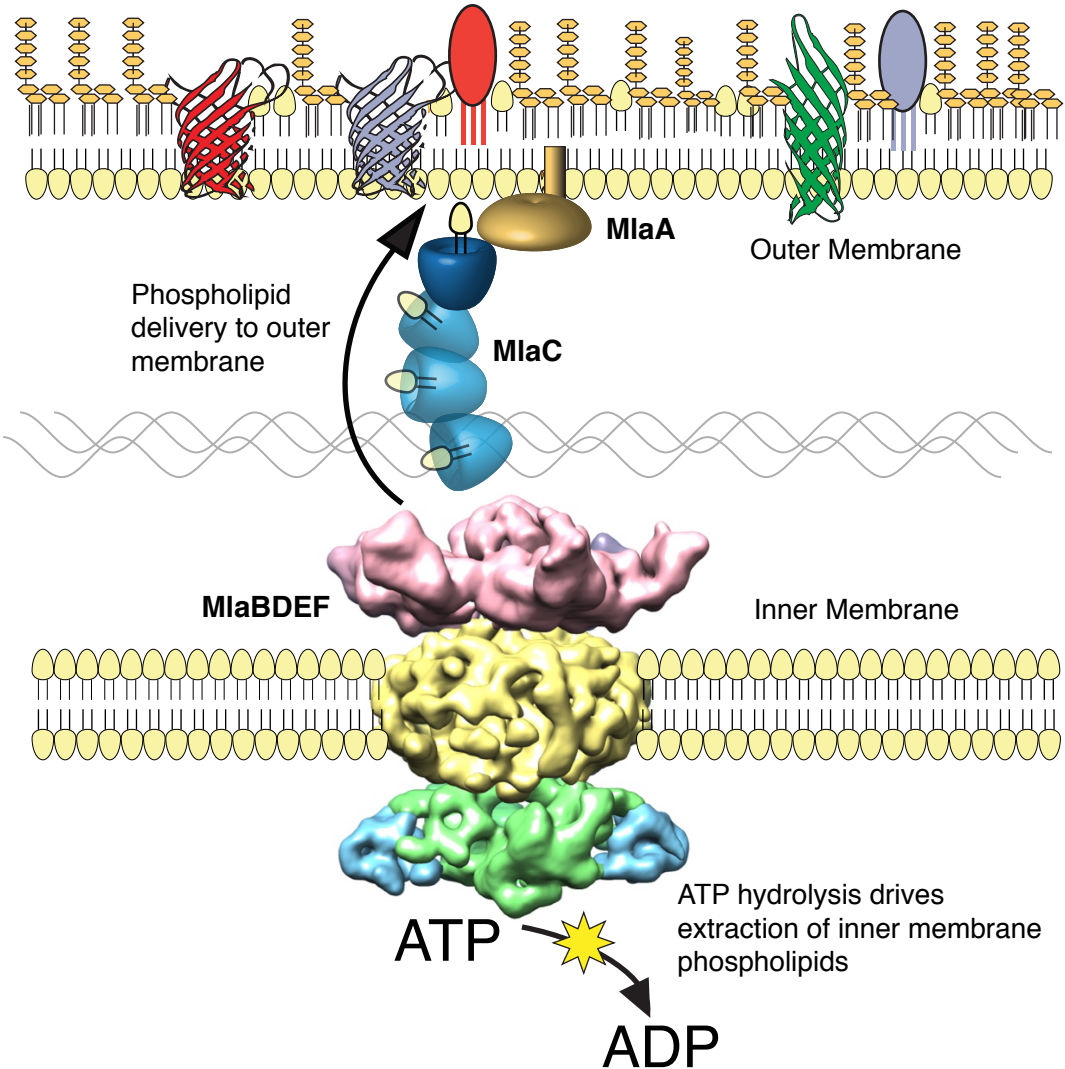

Fig 6. The multicomponent Mla system transports glycerophospholipids from the inner membrane to the outer membrane of *A. baumannii.* A schematic of glycerophospholipid transport to the Gram-negative bacterial outer membrane by the Mla system.